PHYSICAL REVIEW B **77**, 134203 (2008)

Stochastic statistical approach to the kinetics of the first stages of phase separation in alloys

A. Yu. Stroev, I. R. Pankratov, and V. G. Vaks
Russian Research Center "Kurchatov Institute," 123182 Moscow, Russia

(Received 11 September 2007; revised manuscript received 6 January 2008; published 14 April 2008)

The earlier-developed statistical methods for nonequilibrium alloys are generalized to stochastically describe the evolution of microstructure at the first stages of phase separation in alloys. An important parameter of the theory is the size of locally equilibrated regions, which is estimated by using simulations at different values of this parameter. The approach is used to study the microstructural features of both the nucleation and growth (NG) and the spinodal decomposition (SD) types of evolution, as well as the morphological transition NG-SD under variations of c and T across the spinodal curve. We also investigate morphology of precipitates and kinetic features of precipitation at low temperatures. The results obtained agree well with the available experimental observations and Monte Carlo simulations.

DOI: 10.1103/PhysRevB.77.134203 PACS number(s): 05.70.Fh, 05.10.Gg

I. INTRODUCTION

Studies of microstructural evolution in phase-separating alloys attract interest from both fundamental and applied points of view. From the fundamental side, elucidation of microscopic mechanisms for the formation and evolution of embryos of new phases arising under the first-order phase transitions is one of the principal problems in the statistical physics of nonequilibrium systems.[1–3] From the applied side, knowledge of details of microstructure formed by new-born precipitates and elaboration of methods to vary this microstructure are often very important for industrial applications.[4–7]

There are two main kinetic forms of phase separation for an initially homogeneous system quenched into the two-phase equilibrium region: nucleation and spinodal decomposition. For definiteness, we consider the disordered binary alloy A_cB_{1-c} with the concentration-temperature (c,T) phase diagram of the type shown in Fig. 1. There are two important curves in this phase diagram: the two-phase equilibrium curve, or the binodal $T_b(c)$, and the stability limit of the uniform state, or the spinodal $T_s(c)$. According to classical ideas,[2,8,9] in the metastability region $T_s(c)<T<T_b(c)$, the homogeneous phase separation is realized via nucleation and growth (NG) of isolated precipitates of the new phase, while at $T<T_s(c)$, the main kinetic mechanism is the spinodal decomposition (SD) via the development of unstable concentration waves with growing amplitudes. Binder[1] noted that taking into account the fluctuative effects (neglected in the classical theories) should result in some smearing of the borderline between these two evolution types in the c,T plane, though up to now there seems to be "no theoretical approach to describe the behavior in the transition region from SD to NG."[1]

Theoretical studies of microstructural evolution in the phase-separating alloys can be divided into two main classes: those based on some analytical equations describing evolution of nonequilibrium alloys, for brevity to be called "the analytical approaches," and those based on the direct Monte Carlo modeling of these processes, to be called "the Monte Carlo approaches."

Some phenomenological versions of analytical approaches known as "the phase-field method" or "the stochastic phase-field equations" are now widely used in the materials science community (see, e.g., Refs. 10 and 11). However, as discussed in Sec. II B, the phase-field method for alloys can be theoretically justified only near the critical point T_c, which usually has no interest for applications, while the conventional forms of this approach used at other c and T correspond to the numerous arbitrary assumptions discussed in detail in Ref. 12. More importantly, the treatment of fluctuative terms in the stochastic phase-field equations will be shown below to be inconsistent, while attempts to describe the NG-type processes strictly following these equations (which is avoided in actual computations that employ these equations[10,11]) lead to the physically senseless divergent results discussed in Ref. 19 and below. Therefore, this approach cannot be used to study the first stages of phase separation.

More consistent analytical approaches are based on the master equation for probabilities of various atomic distribu-

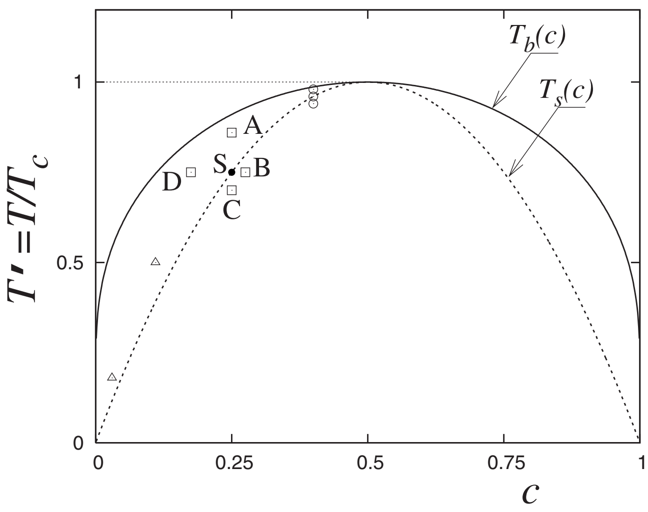

FIG. 1. Concentration-temperature (c,T) phase diagram of a phase-separating alloy calculated in the mean-field approximation. T_c is the critical temperature, $T_b(c)$ is the binodal temperature, and $T_s(c)$ is the spinodal temperature. Circles, squares, and triangles indicate the alloy states chosen for simulations described in Secs. VI B, VI D, and VII, respectively.

tions in a nonequilibrium alloy.[13,14] The statistical development of these ideas based on the generalized Gibbs distribution approach (GGDA) and the quasi-equilibrium kinetic equation (QKE) enables one to adequately describe many peculiar features in the alloy phase transformation kinetics (see Ref. 15 for a review). However, the QKE neglects the fluctuations of atomic fluxes violating the second law of thermodynamics,[16,17] while the presence of such fluctuations is crucial for the first stages of nucleation or for the spinodal decomposition near the spinodal curve. To describe these processes, the QKE should be generalized to allow for such fluctuations.

The most reliable theoretical information about the first stages of nucleation is presently provided by the Monte Carlo modeling, in particular, by simulations based on the kinetic Monte Carlo approach (KMCA).[3–5] A number of microstructural features of nucleation have been found in these studies and confirmed by the atomic-resolution experiments.[4,5] However, applications of the KMCA to more broad studies of phase separation in alloys are limited for a number of reasons. First, the elastic strain effects important for many phase-separating alloys cannot be easily taken into account in the KMCA, while it makes no problem for the statistical approaches.[15] Second, the KMCA is well suited to simulate the first stages of nucleation, while to describe the next longer stages of evolution, it should be conjugated to some analytical approach, such as the cluster dynamics method used in Ref. 5. Such conjugation can be made more or less unambiguously only for the well-separated precipitates. It corresponds to the nucleation processes at c, T values far enough from the spinodal curve, while describing the phase separation near or within this curve here meets difficulties. For these, as well as for many other reasons, the direct Monte Carlo modeling, in spite of its evident achievements and value, cannot replace the consistent statistical theory of evolution of microstructure under phase separation.

This work is an attempt to develop such a theory by using the stochastic generalization of the QKE mentioned above. To describe fluctuations of diffusion fluxes disregarded in the QKE, we use the "Langevin-noise-type" approach, which is often employed to simulate the influence of fluctuations on evolution in mechanical systems. To properly apply this approach to our statistical problem, we should thoroughly analyze the basic notions of statistical theories of nonequilibrium systems. This analysis leads to the appearance in the theory of an important kinetic parameter, the characteristic size of locally equilibrated regions, which can be estimated by using simulations of microstructural evolution for the different values of this parameter. The resulting equations provide the stochastic statistical description of evolution of atomic distributions in a nonequilibrium alloy. The methods developed are applied to studies of some concrete problems in the phase separation kinetics.

The paper is organized as follows. In Sec. II, we present the basic relations of GGDA needed in what follows. In Sec. III, we discuss the problem of incorporating the fluctuative terms into the statistical description of nonequilibrium systems. In Sec. IV, we formulate the basic equations of our stochastic approach, while in Sec. V, we present its "continuous" version that can be used when all characteristic lengths of the problem much exceed the interatomic distance, in particular, at c, T values near the critical point. In Sec. VI, we apply the methods developed to study the morphological transition NG-SD for a number of concentrations, temperatures, and alloy models. In Sec. VII, we investigate morphology of precipitates and kinetic features of precipitation at low temperatures. The main conclusions are presented in Sec. VIII. Some preliminary results of this work have been reported earlier.[18–20]

II. QUASIEQUILIBRIUM KINETIC EQUATION

A. Quasiequilibrium kinetic equation for the discrete lattice

Let us first present the main equations of GGDA disregarding the fluctuative effects. We consider the substitutional alloy A_cB_{1-c}. Various distributions of atoms over lattice sites i are described by the sets of occupation numbers $\{n_i\}$, where the operator $n_i=n_{Ai}$ is unity when site i is occupied by atom A and zero otherwise. The interaction Hamiltonian H has the form

$$H=\sum_{i>j} v_{ij}n_in_j, \tag{1}$$

where v_{ij} are effective interactions supposed to be pairwise for simplicity.

The GGDA is based on the master equation for the probability P to find the occupation number set $\{n_i\}=\xi$,

$$dP(\xi)/dt=\sum_{\eta}\,[W(\xi,\eta)P(\eta)-W(\eta,\xi)P(\xi)], \tag{2}$$

where $W(\xi,\eta)$ is the $\eta\to\xi$ transition probability per unit time for which we use the conventional thermally activated direct-atomic-exchange model.[15] As discussed in detail in Refs. 12 and 15, for the usual conditions of phase transformations, the probability P in Eq. (2) can be written in the following "quasiequilibrium" form:

$$P\{n_i\}=\exp\left[\beta\left(\Omega+\sum_i \lambda_i n_i-\sum_{i>j} v_{ij}n_in_j\right)\right]. \tag{3}$$

Here, β is $1/T$, the parameters λ_i (being, generally, both time and space dependent) can be called the "site chemical potentials," and the constant $\Omega=\Omega\{\lambda_i\}$ is determined by the normalization.

Multiplying Eq. (2) by the operator n_i and summing over *all* configurational states (which implies neglecting the fluctuative contributions discussed below), we obtain the QKE,[15]

$$dc_i/dt=\sum_j M_{ij}2\sinh[\beta(\lambda_j-\lambda_i)/2]. \tag{4}$$

Here, the mean site occupation c_i corresponds to averaging the operator n_i over distribution [Eq. (3)],

$$c_i=\bar{n}_i=\sum_{\{n_j\}} n_iP\{n_j\}, \tag{5}$$

and the "generalized mobility" M_{ij} is a similar average of some other function of occupation numbers.[15] To explicitly find functions $\lambda_i\{c_j\}$ and $M_{ij}\{c_k\}$ in Eqs. (4) and (5), we should use some method of statistical calculations. For example, in the simplest, "kinetic mean-field" approximation (KMFA), we obtain[15]

$$\lambda_i = T\ln(c_i/c_i') + \sum_j v_{ij}c_j, \tag{6}$$

$$M_{ij} = \gamma_{ij}[c_i c_i' c_j c_j' \exp(\beta u_i + \beta u_j)]^{1/2}, \tag{7}$$

where c_i' is $(1-c_i)$, γ_{ij} is the configuration-independent factor in the probability of an intersite atomic exchange per unit time defined in Ref. 15, and u_i is the "asymmetrical potential"[13] supposed below to be zero. If, to calculate $\lambda_i\{c_j\}$ and $M_{ij}\{c_k\}$ in Eq. (4), we employ a more refined method than the KMFA, e.g., the kinetic cluster methods,[15] basic Eq. (4) retains its form but functions $\lambda_i(c_j)$ and $M_{ij}(c_k)$ are given by more complex expressions. This difference seems to be unessential for what follows, the more so that the differences between the MFA and the cluster method results for the disordered phase-separating alloys are usually small (unlike, for example, the case of the fcc alloys with $L1_2$- or $L1_0$-type orderings where employing the cluster methods is necessary[15]). Therefore, for simplicity, below we use the KMFA expressions (6) and (7).

Let us also note that Eqs. (4)–(7) correspond to employing the simplified "direct-atomic-exchange" model instead of the more realistic vacancy-mediated atomic exchange model used in more quantitative treatments.[3–5] However, due to the "equivalence theorem" discussed in Ref. 17, this simplification does not seem to be essential for the most of problems discussed in this paper.

For further generalizations, it is also convenient to rewrite the QKE [Eq. (4)] in the "finite difference" form, integrating it over a small time interval δt,

$$\delta\bar{n}_i = \sum_j M_{ij} 2\sinh[\beta(\lambda_j - \lambda_i)/2]\delta t, \tag{8}$$

where we use the full notation $\bar{n}_i$ instead of the shortened one, c_i.

B. Quasiequilibrium kinetic equation in the continuous approximation

When the space variations of local occupations $c_i = c(\mathbf{R}_i)$ are smooth, that is, when the smallest inhomogeneity length $l_{\rm inh}$ (which in our problem is the interphase boundary width $w_{\rm ipb}$) much exceeds the interatomic distance d, we can expand Eqs. (4)–(7) in powers of ∇c. This approximation, which corresponds to the generalized Ginzburg–Landau[12] or the Cahn–Hilliard[21] approach, will be called below as the "continuous" approximation. Physically, this approximation is always valid at high temperatures T near the critical temperature T_c, as the interphase boundary width here is large. For example, in the MFA used, $w_{\rm ipb}$ rises at $T\to T_c$ as $(T_c - T)^{-1/2}$. At arbitrary temperatures, the continuous approximation can be true if the interaction range notably exceeds the interatomic distance.[12] For metallic alloys, such extended interactions are generally not typical, but they can be present in some polymer mixtures.[1]

In the continuous approximation, Eqs. (4)–(7) for cubic alloys (e.g., fcc or bcc ones) take the following form:[22]

$$dc/dt = \mathrm{div}[M(c)\beta\nabla\lambda(c)], \tag{9}$$

$$\lambda(c) = T\ln(c/c') - 4T_c[c + (r_0^2/6)\nabla^2 c], \tag{10}$$

$$M(c) = \gamma c c'. \tag{11}$$

Here, γ is $\frac{1}{6}\Sigma_j \gamma_{ij} r_{ij}^2$ with $r_{ij} = |\mathbf{R}_i - \mathbf{R}_j|$, $T_c = (-\Sigma_j v_{ij}/4)$ is the critical temperature in the MFA, and $r_0^2 = \Sigma_j v_{ij} r_{ij}^2/\Sigma_j v_{ij}$ is the mean interaction radius squared. For the nearest-neighbor-atomic-exchange model used below with $\gamma_{ij} = \gamma_{nn}$, the value of γ in Eq. (11) for cubic alloys is $\gamma_{nn}a^2$, where a is the fcc or the bcc lattice constant. Equations (9) and (10) show, in particular, that within the continuous approximation and the MFA used, the configurational interaction in an alloy is fully characterized by its mean interaction radius r_0, while the critical temperature T_c determines its scale.

To proceed from the continuous QKE [Eq. (9)] to its finite difference version similar to Eq. (8), we rewrite this equation in the "discrete" form. To this end, we divide the lattice into the cubic cells of size L (L cells). Each L cell centered at the point $\mathbf{R}_i$ ("cell i") is supposed to include a sufficiently large number of lattice cites equal to $N_L = 4L^3/a^3$ for the fcc lattice or $N_L = 2L^3/a^3$ for the bcc lattice: $N_L \gg 1$. At the same time, the size L is supposed to be much less than the characteristic inhomogeneity length $l_{\rm inh} \sim w_{\rm ipb}$,

$$1 \ll N_L, \quad L \ll w_{\rm ipb}. \tag{12}$$

These two inequalities are evidently compatible only when $w_{\rm ipb} \gg a$, i.e., when the continuous approximation is valid.

Then, we sum Eq. (9) over all sites j within the cell i, thus obtaining on the left-hand side $d\bar{N}_i/dt$, where $\bar{N}_i = \Sigma_j c_j$. On the right-hand side, we approximate the sum over j by the volume integral over cell i, and then transform it into surface integrals over six facets s of cell i. Integrating the result over a small time interval δt, we obtain the finite difference version of Eq. (8),

$$\delta\bar{N}_i = \sum_{s=1}^{6} (L^2/v_a)\mathbf{n}_s \beta(M\nabla\lambda)_s \delta t. \tag{13}$$

Here, v_a is the atomic volume, $\mathbf{n}_s$ is the unit vector normal to the facet s directed off the cell i, the gradient term $\nabla\lambda$ for the cell j adjacent to cell i can be approximated by the appropriate finite difference, and the mean local occupation c_i in the functions $M(c_i)$ and $\nabla\lambda\{c_i\}$ is approximated as $c(\mathbf{R}_i) = \bar{N}_i/N_l$.

As mentioned, the mesh size L in Eq. (13) should satisfy to both inequalities [Eq. (12)]. In our simulations of phase separation near the critical point, we employ $L=2a$ or $L=1.5a$, where a is the fcc lattice constant. As discussed in Sec. VI B, the continuous approximation with these L can be safely used for such simulations.

III. FLUCTUATIVE TERMS AND STOCHASTIC EQUATIONS

Let us discuss the relation between the quantities $c_i = \bar{n}_i$ or $\bar{N}_i$ entering Eqs. (4) and (8), or (13) and the concentration distribution $c_{\rm obs}(\mathbf{R},t)$ observed experimentally. Note that the

GGDA, being a statistical approach based on “ensemble averages” $c_i = \bar{n}_i$, is physically informative and complete only for a “macroscopically” nonequilibrium system (see, e.g., Ref. 8, Sec. VII) that can be divided into some locally equilibrated quasiclosed subsystems with the size l_{le} much exceeding the interatomic distance d. Within each subsystem, the site chemical potential λ_i is approximately constant, and its fluctuations have a relative scale $(d/l_{\mathrm{le}})^{3/2} \ll 1$. Therefore, the summation over alloy states in Eq. (5) should include not all distributions $\{n_i\}$ but only those with the limited inhomogeneity lengths $l < l_{\mathrm{le}}$, while the long-wave fluctuations with $l \gtrsim l_{\mathrm{le}}$ remain to be fixed in the macroscopically nonequilibrium state under consideration. Therefore, the “diffusive” term in the right-hand side of Eqs. (4), (8), and (13), corresponds just to a “coarse-grained” averaging in Eq. (5) performed at the fixed distribution of these long-wave fluctuations, and the terms allowing for their dynamics should also be considered to describe the full $c_{\mathrm{obs}}(\mathbf{R},t)$. These fluctuative terms were neglected in the previous GGDA-based treatments of phase transformations[15] as usually they have little effect on evolution. However, for the phase separation above and near the spinodal curve, the presence of such terms is crucial.

We describe these fluctuative terms by using the stochastic Langevin-type approach. To this end, we proceed from the average $\bar{n}_i = c_i$ to an “individual phase trajectory,” that is, to the actual occupation number $n_i(t)$ at site i. It differs from the average $\bar{n}_i(t)$ due to the fluctuations of the atomic transfer δn_{fs} through each bond $s = \{i,j\}$ that connects the site i with some of its neighbor j and along which the unlike neighboring atoms at sites i and j can interchange their positions (for the direct-atomic-exchange model used). Therefore, instead of Eq. (8), we have the following expression for the change of the occupation n_i for the time interval δt:

$$\delta n_i \equiv n_i(t+\delta t) - n_i(t) = \delta n_{di}\{c_j\} + \sum_j \delta n_{fs}. \tag{14}$$

Here, the diffusive term δn_{di} is given by the right-hand side of Eq. (8), and the sum of fluctuative atomic transfers δn_{fs} is taken over all bonds $s = \{i,j\}$ that connect site i with its neighbors j.

Following Langevin’s idea,[23] we treat each fluctuative transfer δn_{fs} as a random quantity with the Gaussian probability distribution

$$W(\delta n_{fs}) = A_s \exp(-\delta n_{fs}^2 / 2D_s), \tag{15}$$

where A_s is the normalization constant and the dispersion D_s is the same as that for the actual fluctuative transfer δn_{fs}.

The D_s value can be found as follows. Let us denote for brevity the total atomic transfer from site j to site i through the bond $s = \{i,j\}$ as δn_s and the quantity $\exp[\beta(\lambda_j - \lambda_i)/2]$ in Eq. (8) as x. For a small time interval δt under consideration, the transfer δn_s takes either of three values: 0, 1, or -1. One can also see from the derivation of the QKE [Eq. (4)] given in Ref. 15, that the term $M_{ij} x \delta t$ in Eq. (8) is the probability W_1 to find the value $\delta n_s = 1$, while the term $M_{ij}\delta t / x$ is the probability W_{-1} to find the value $\delta n_s = -1$. Thus, for the statistical averages $\langle \delta n_s \rangle$ and $\langle \delta n_s^2 \rangle$, we obtain

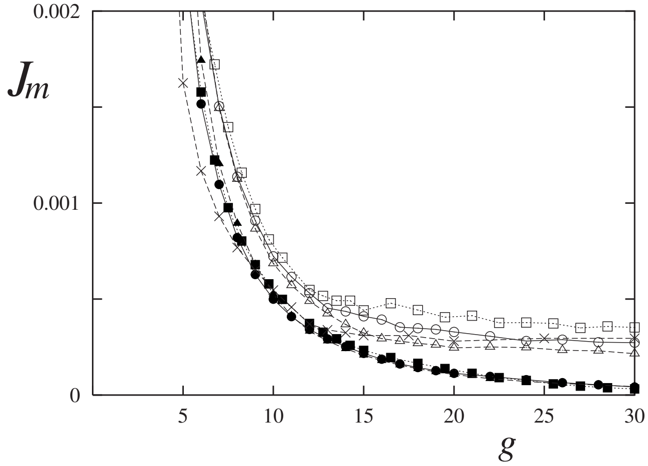

FIG. 2. The inhomogeneity parameter $J_m(g)$ described in the text versus the cutoff parameter $g = l/a$ for 2D simulations discussed in Secs. VI B and VI C at $t_e = 5 \cdot 10^4 / \gamma_{nn}$ and $c = 0.4$. Squares, circles, and triangles correspond to the fcc alloy model with the reduced mean interaction radius $r_0' = r_0/a$ equal to 0.707, 1, and 2, respectively, treated in the continuous approximation [Eqs. (27)–(32)]. Closed symbols correspond to the reduced temperature $T' = T/T_c = 0.98$, and open symbols to $T' = 0.94$. Crosses correspond to the discrete lattice approach [Eqs. (19)–(24)] for the fcc-3 model at $T' = 0.94$ discussed in Sec. VI B.

$$\langle \delta n_s \rangle = W_1 - W_{-1}, \quad \langle \delta n_s^2 \rangle = W_1 + W_{-1}. \tag{16}$$

The first equation in Eq. (16) is evidently equivalent to the QKE [Eq. (8)]. In the general expression for the dispersion of the atomic transfer,

$$\langle \delta n_{fs}^2 \rangle = \langle (\delta n_s - \langle \delta n_s \rangle)^2 \rangle = \langle \delta n_s^2 \rangle - \langle \delta n_s \rangle^2, \tag{17}$$

the first term is given by the second equation in Eq. (16), while the second term has the second order in δt and can be neglected. Therefore, the dispersion D_s can be expressed via quantities that enter the QKE [Eq. (8)],

$$D_s = \langle \delta n_{fs}^2 \rangle = 2M_{ij}\delta t \cosh[\beta(\lambda_j - \lambda_i)/2]. \tag{18}$$

As mentioned, the site chemical potential λ_i is approximately constant within each locally equilibrated quasiclosed subsystem. Therefore, the difference $(\lambda_j - \lambda_i)$ for the adjacent sites i and j is typically small, and the argument of cosh in Eq. (18) is much less than unity. It is illustrated by Figs. 2–4 characterizing the scale of quantities $\beta|\lambda_j - \lambda_i|$ averaged according to Eqs. (25) and (26). Thus, the last factor in Eq. (18) in our calculations was omitted (though the special case of very low temperatures, when the products $\beta|\lambda_j - \lambda_i|$ cannot be small even though the differences $|\lambda_j - \lambda_i|$ are small, may need a separate consideration). In the KMFA used, the mobility M_{ij} in Eq. (18) is given by Eq. (7).

Let us now discuss which quantities c_j should be used as the arguments for the local chemical potential $\lambda_i\{c_j\}$ and the local mobility $M_{ij}\{c_k\}$ in the diffusive term δn_{di} in Eq. (14). The most “natural” (but naive) prescription seems to be just to replace here c_j by $n_j(t)$, that is, to put $\lambda_i\{c_j\} \to \lambda_i\{n_j(t)\}$ and $M_{ij}\{c_k\} \to M_{ij}\{n_k(t)\}$. It corresponds to the treatment of fluctuations of both the occupation number n_i and the chemical

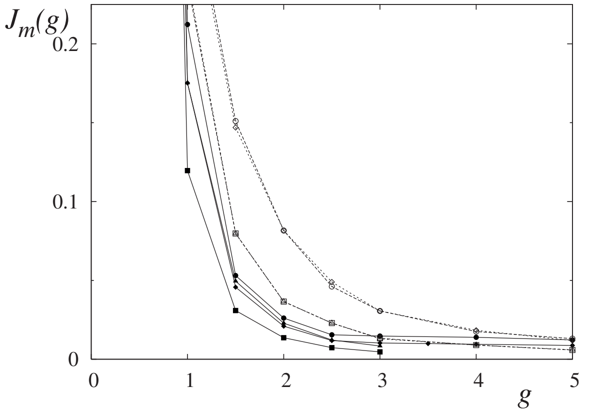

FIG. 3. Same as in Fig. 2 for the simulations described in Sec. VI B at $t_e = 10^4/\gamma_{nn}$. Open symbols correspond to 2D simulations at $c = 0.25$ and the following models and temperatures: squares, bcc-1, $T' = 0.86$; triangles, bcc-3, $T' = 0.86$; circles, bcc-1, $T' = 0.7$; rhombuses, bcc-3, $T' = 0.7$. Solid symbols correspond to 3D simulations for the bcc-1 model at the following concentrations and temperatures: squares, $c = 0.25$, $T' = 0.86$; circles, $c = 0.25$, $T' = 0.7$; triangles, $c = 0.175$, $T' = 0.75$; rhombuses, $c = 0.275$, $T' = 0.75$.

potential λ_i (or the mobility M_{ij}) on the same footing, and just this recipe is declared in the stochastic phase-field treatments of phase separation.[10,11] However, the numerical realization of this "direct" recipe leads to the physically senseless results, namely, to totally chaotic evolution with no hints of a tendency to the thermodynamic equilibrium of any kind at any T and c. It is illustrated, in particular, by Fig. 2 in Ref. 19.

Let us note that in the actual computations using the "stochastic phase-field" equations,[10,11] the fluctuative terms were switched on after a short initial period. Thus, overestimating these terms mentioned above leads just to the distortion of evolution for this short period and to the wrong distribution of precipitates at its end, but the further evolution (treated using the QKE-type equations[12]) can be described more or less properly.

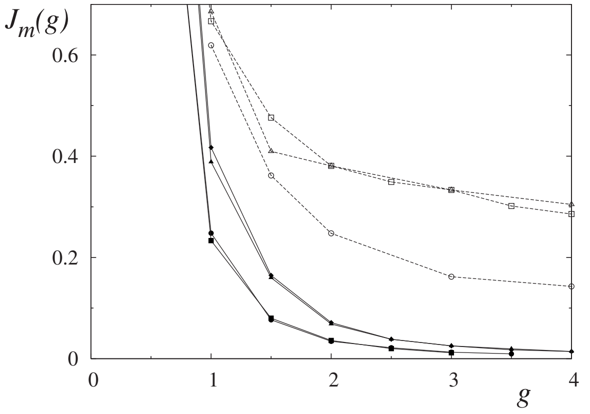

FIG. 4. Same as in Fig. 2 for 3D simulations described in Sec. VII at $t_e = 10^4/\gamma_{nn}$. Solid symbols correspond to the simulations at $c = 0.11$, $T' = 0.5$, and the following models: squares, fcc-1; circles, fcc-3*b*; triangles, bcc-1; rhombuses, bcc-3*a*. Open symbols correspond to the bcc-1 model and the following concentrations and temperatures: squares, $c = 0.03$ and $T' = 0.18$; circles, $c = 0.1$ and $T' = 0.3$; triangles, $c = 0.2$ and $T' = 0.3$.

If one arbitrarily decreases the fluctuation scale D_s in Eqs. (14)–(18) by 1–2 orders of magnitude, the evolution becomes to look more plausible, as illustrated in Fig. 2 in Ref. 19. However, there seems to be no arguments for such drastic reducing of fluctuations within this direct approach.

The physical origin of the failure of such a direct approach is the fundamental difference between the fluctuations of the "mechanistic" quantities n_i having a direct and measurable meaning and the fluctuations of the "thermodynamic" quantities λ_i describing the locally equilibrated quasiclosed subsystems. As mentioned, expression (8) for the diffusive term is obtained by the statistical averaging over all fluctuations of occupations $\{n_j\}$ except for those with the large wavelengths l exceeding the length l_{le} of a local equilibrium. Thus, it makes no sense to include again the short-wave fluctuations with $l < l_{\text{le}}$ in the diffusive term δn_{di} that has been already averaged over these fluctuations. The fluctuation of the parameter λ_i in Eq. (3) can have a physical meaning only if it takes an approximately identical value for the whole volume $V_{\text{le}} \sim l_{\text{le}}^3$, that is, if it has a wavelength $l \gtrsim l_{\text{le}} \gg d$.

In other words, the total fluctuative transfer δn_{fs} through each bond s described by Eqs. (15)–(18) is by no means small. However, the main short-wave contribution of these fluctuations to the microstructural evolution is self-averaging and is described by the diffusive term δn_{di}. Only the long-wave fluctuations with $l \gtrsim l_{\text{le}}$ remain meaningful for this term and should be taken into account in the calculations.

IV. COARSE-GRAINED DESCRIPTION: FILTRATION OF NOISE

To describe this physical picture, we suggest the following model. Instead of the full stochastic quantities $n_i(t)$ and δn_{di} in Eq. (14), we consider only their long-wave parts, $n_i^c(t)$ and δn_{di}^c, determined by a coarse-grained version of Eq. (14),

$$n_i^c(t+\delta t) = n_i^c(t) + \delta n_{di}\{c_j\} + \sum_j \delta n_{fs}^c, \tag{19}$$

where all arguments c_j in the diffusive term δn_{di} [given by the right-hand side of Eq. (8)] are substituted by $n_j^c(t)$. To define the coarse-grained fluctuative transfer δn_{fs}^c, we divide all bonds s into several equivalent bond sublattices α. Each of them includes all bonds with the same orientation α, and lattice sites in this sublattice are positioned at the bond centers $\mathbf{R}_{s\alpha}$. For the fcc alloy, there are six such fcc sublattices with the bonds oriented along (1,1,0), (1,−1,0), (0,1,1), (0,1,−1), 1,0,1), or (1,0,−1), while for the bcc alloy, there are four bcc bond sublattices with the bonds along (1,1,1), (−1,1,1), (1,−1,1), or (1,1,−1). Then, the last terms in Eqs. (14) and (19) take the forms

$$\sum_j \delta n_{fs} = \sum_{j,\alpha} \delta n_{f\alpha}(\mathbf{R}_{s\alpha}), \tag{20}$$

$$\sum_j \delta n_{fs}^c = \sum_{j,\alpha} \delta n_{f\alpha}^c(\mathbf{R}_{s\alpha}). \tag{21}$$

The coarse-grained fluctuative transfer $\delta n^c_{f\alpha}(\mathbf{R}_{s\alpha})$ in the last term of Eq. (21) is obtained from the full stochastic distribution $\delta n_{f\alpha}(\mathbf{R}_{s\alpha})$ determined by Eqs. (15)–(20) by a "filtration of noise" procedure, that is, by introducing a proper cutoff factor $F_c(\mathbf{k})$ in the Fourier component $\delta n_{f\alpha}(\mathbf{k})$ of the full function $\delta n_{f\alpha}(\mathbf{R}_{s\alpha})$,

$$\delta n^c_{f\alpha}(\mathbf{R}_{s\alpha}) = \sum_{\mathbf{k}} \exp(-i\mathbf{k}\mathbf{R}_{s\alpha})\delta n_{f\alpha}(\mathbf{k})F_c(\mathbf{k}),$$

$$\delta n_{f\alpha}(\mathbf{k}) = \frac{1}{N}\sum_{\mathbf{R}_{s\alpha}} \exp(i\mathbf{k}\mathbf{R}_{s\alpha})\delta n_{f\alpha}(\mathbf{R}_{s\alpha}), \qquad (22)$$

where N is the total number of lattice sites (or atoms). The factor $F_c(\mathbf{k})$ should sharply decrease at k exceeding some characteristic reciprocal length $1/l \sim 1/l_c$. We also should remember that the bond centers $\mathbf{R}_{s\alpha}$ at each α form a crystal lattice similar to that of cites i. Thus, the Fourier component $\delta n^c_{f\alpha}(\mathbf{k})$ should have the proper crystal symmetry and should not change under adding any reciprocal lattice vector to $\mathbf{k}$. For simplicity, we take the factor $F_c(\mathbf{k})$ in the following form:

$$F_c(\mathbf{k}) = \exp\left[-g^2\sum_n (1-\cos \mathbf{k}\mathbf{R}_{1n})/2\right]. \qquad (23)$$

Here, $\mathbf{R}_{1n}$ are the first-neighbor lattice vectors in the fcc or the bcc lattice, the sum is taken over all such vectors, and at large $g^2 \gg 1$ used below, expression (23) is reduced to a Gaussian $\exp(-k^2l^2/2)$ with $l=ga$. The explicit forms of Eq. (23) for the fcc or the bcc lattice are

$$F_c^{\text{fcc}}(\mathbf{k}) = \exp[-2g^2(3-\cos\varphi_1\cos\varphi_2-\cos\varphi_2\cos\varphi_3 - \cos\varphi_3\cos\varphi_1)],$$

$$F_c^{\text{bcc}}(\mathbf{k}) = \exp[-4g^2(1-\cos\varphi_1\cos\varphi_2\cos\varphi_3)], \qquad (24)$$

where $\varphi_\alpha = k_\alpha a/2$, k_α is the vector $\mathbf{k}$ component along the main crystal axis α, and a is the fcc or the bcc lattice constant.

Equation (19) with the fluctuative terms δn^c_{fs} defined by relations (22)–(24) will be called below as "the stochastic kinetic equation" (SKE). It differs from the QKE by the presence of fluctuative terms δn^c_{fs}.

The "true" cutoff length $l=l_c$ for our problem should have the order of a characteristic local equilibrium length l_{le}, that is, the minimal size for which the local equilibrium notion and thus local thermodynamic potentials, in particular, site chemical potentials λ_i entering Eqs. (3) and (4), can be introduced for the process under consideration: phase separation can take place only when a sufficient thermodynamic driving force (i.e., supersaturation) is present, which implies a certain extent of the local thermodynamic equilibrium within a quasiclosed subsystem. At the same time, all fluctuations with the larger wavelengths $l \gtrsim l_{\text{le}}$ can initiate this process and thus should be taken into account. The length l_{le} can generally depend on the concentration c, temperature T, and the interatomic interactions v_{ij}. To estimate the l_{le} value, we made computer simulations of phase separation based on Eqs. (19)–(24) for a number of different models, concentrations, and temperatures while varying the parameter $g=l/a$ in Eq. (24). In accordance to the considerations above, the decrease of l from the values $l>l_{\text{le}}$ to $l<l_{\text{le}}$ should correspond to the loss of the local equilibrium assumed in Eqs. (3)–(7) and, thus, to sharp violations of the basic condition $\lambda_i \simeq \text{const}$ within quasiclosed subsystems.

TABLE I. Values of reduced interactions $v'_n = v_n/v_1$ for some alloy models used in Secs. VI and VII.

Model	v'_2	v'_3	Model	v'_2	v'_3
fcc-3	0.8	0.5	bcc-3	0.5	0.25
fcc-3*a*	0.5	−0.158	bcc-3*a*	0.5	−0.309
fcc-3*b*	0.5	−0.208			

The scale of these violations at the given evolution time t can be characterized, for example, by the value of the reduced difference of chemical potentials of neighboring sites averaged over the whole system,

$$J(g,t) = \frac{1}{N_b}\sum_{s=\{i,j\}} |\lambda_i - \lambda_j|\beta, \qquad (25)$$

where N_b is the total number of bonds, and the summation is made over all bonds $s=\{i,j\}$. Then, the "degree of nonequilibrium" for the whole evolution, or the inhomogeneity parameter $J_m(g)$, can be defined as the maximum value of the quantity $J(g,t)$ in Eq. (25) for some characteristic evolution time t_e,

$$J_m(g) = [J(g,t<t_e)]_{\max}. \qquad (26)$$

Then, decreasing $l=ga$ across l_{le} should result in a sharp rise of $J_m(g)$. This is illustrated in Figs. 2–4 calculated for various alloy models discussed below. The point g_{sr} where this sharp rise starts can be defined, for example, as the maximum curvature point for the function $J_m(g)$. The local equilibrium length $l_{\text{le}} \simeq l_c = g_c a$ should evidently somewhat exceed the $l_{sr}=g_{sr}a$ value and should correspond to the values of g at which the curvature of $J_m(g)$ becomes small. The experience of our simulations shows that employing $g_c \simeq 2g_{\text{sr}}$ usually provides an appropriate description of evolution, while varying g_c, say, between $2g_{\text{sr}}$ and $1.5g_{\text{sr}}$ results mainly in some rescaling of time and only slight changes of microstructure. It is illustrated below by comparison of frames 6(b) and 6(e) to 6(g) and 6(h) or frames 7(a), 7(b), and 7(c) to 7(d), 7(e) and 7(f).

In Figs. 2–4, we present the dependence $J_m(g)$ for various alloy models used in our simulations. In these figures, symbol fcc-1 or bcc-1 means the fcc or the bcc alloy model with the nearest-neighbor interaction $v_1<0$; symbol fcc-3, fcc-3*a*, fcc-3*b*, bcc-3, or bcc-3*a* means the three-neighbor-interaction model on the fcc or the bcc lattice with $v_1<0$ and the reduced interactions $v'_n = v_n/v_1$ given in Table I; symbol "fcc, r'_0=0.707, 1, or 2" means the fcc alloy model treated in the continuous MFA described in Sec. II at the value $r'_0 = r_0/a$ indicated. In Table II, we present the cutoff values $g_c = l_c/a$ used in our simulations.

Let us discuss the results shown in these figures and tables. Figure 2 corresponds to the (c,T) values near the critical point, Fig. 3 to the intermediate temperatures T'

TABLE II. Values of cutoff parameter $g=g_c$ in Eqs. (24) and (32) used in our simulations.

Dimension	2D		3D	
Alloy model	fcc at $r_0'=0.7,1$ and 2, fcc-3	bcc-1, bcc-3	fcc-1, fcc-3*a*, fcc-3*b*, bcc-1, bcc-3*a*	bcc-1
Concentration c	0.4	0.25	0.1–0.2	0.03
$T'=T/T_c$	0.94–0.98	0.7–0.86	0.3–0.5	0.18
g_c	20–26	5	3	3

$=0.7-0.9$, and Fig. 4 to the lower temperatures $T'\lesssim 0.5$. The figures illustrate the general features of functions $J_m(g)$ mentioned above. At large g, these functions flattens, while at g below some g_{sr}, they start to sharply rise, which reflects the loss of local equilibrium at $l=ga<l_{\mathrm{le}}$. The detailed form and the scale of these functions strongly vary with the concentration c and temperature T, particularly when these variations correspond to crossing the spinodal curve in the (c,T) plane, which implies the change of the evolution type from NG to SD. In the physically interesting region $g\gtrsim g_c$, the $J_m(g)$ values in the SD field of the (c,T) plane typically exceed those in the NG field by several times. A more detailed analysis shows that the maximum values $J(g,t)$ in Eq. (26) at SD are usually attained at first stages of precipitation when the unstable concentration waves start to interact with each other,[15,22] while for the NG-type evolution, this maximum typically corresponds to the beginning of the growth stage. For both types of evolution, the maximum values of differences $|\lambda_i-\lambda_j|$ in Eq. (25) are attained at the precipitate-matrix interfaces. With lowering T, the $J_m(g)$ values in the physically interesting region $g\gtrsim g_c$ notably increase, which reflects an increase of thermodynamic driving forces proportional to the factors $\beta|\lambda_i-\lambda_j|$ in the QKE [Eq. (4)]. It is illustrated, in particular, by dashed curves in Fig. 3. At the same time, sensitivity of $J_m(g)$ to the interaction type appears to be weak. For example, the $J_m(g)$ values for the bcc-1 and the bcc-3 models in Fig. 3, as well as those for the bcc-1 and the bcc-3a or the fcc-1 and the fcc-3b models in Fig. 4, do almost coincide with each other, even though some thermodynamic and kinetic characteristics within each of these pairs of alloy systems differ notably (see Sec. VII). Solid symbols and curves in Fig. 4 also show that at the similar values of thermodynamic parameters, the scale of fluctuations in bcc alloys exceeds that in the fcc alloys; it can be related to the less dense atomic packing in the bcc structure, as compared to the fcc structure.

Figures 2 and 3 and Table II illustrate the well-known effects of a sharp increase of both the fluctuation effects and the local equilibrium length with approaching the critical point. They also demonstrate the larger scale and the stronger manifestations of these fluctuations in two-dimensional (2D) systems as compared to three-dimensional (3D) systems. In particular, the value $l_{\mathrm{le}}/a\simeq g_c=5$ in the second column of Table II (which corresponds to the 2D systems outside the critical region) is by 4–5 times smaller than $g_c=20-26$ in the first column (which corresponds to the 2D systems within the critical region), but it is by 1.5–2 times larger than the value $g_c=3$ in the third column (which corresponds to the 3D systems far from T_c). At the same time, Figs. 2–4 and Table II show that for the most interesting case of 3D alloys outside the critical region, the size of locally equilibrated regions in the kinetic processes under consideration remains to be approximately the same for all concentrations, temperatures, and interaction types studied in this work, $l_{\mathrm{le}}\simeq 3a$, and the scale of this size seems to be physically reasonable.

V. STOCHASTIC KINETIC EQUATION IN THE CONTINUOUS APPROXIMATION

Employing the continuous approximation mentioned in Sec. II and used in Refs. 18 and 19 enables us to greatly simplify treatments of phase separation near the critical point where all characteristic lengths are large. In this approximation, instead of the site occupation n_i entering Eq. (14), we consider the total number of A atoms within an L cell, N_i, defined in Sec. II and used in Eq. (13). Thus, the "continuous" version of Eq. (14) takes the form

$$\delta N_i \equiv N_i(t+\delta t) - N_i(t) = \delta N_{\mathrm{di}}\{c_j\} + \delta N_{fi}. \tag{27}$$

Here, the diffusive term δN_{di} is given by the right-hand side of Eq. (13) and the fluctuative term δN_{fi} is $\Sigma_s \delta N_{fs}$, where δN_{fs} is the fluctuation of the atomic transfer across facet s for the time interval δt.

Following again Langevin's idea,[23] we treat each fluctuative transfer δN_{fs} as a random quantity with the Gaussian probability distribution. Then, instead of Eqs. (15) and (18), we obtain the similar relations for the fluctuative atomic transfer across facet s,

$$W(\delta N_{fs}) = A_s \exp(-\,\delta N_{fs}^2/2D_{sN}), \tag{28}$$

and the KMFA calculation of the dispersion D_{sN} yields

$$D_{sN} = \langle \delta N_{fs}^2\rangle = \gamma_{nn}\delta t N_b 2c_s(1-c_s), \tag{29}$$

where N_{bs} is the total number of bonds crossed by the facet s equal to $8L^2/a^2$ for the fcc lattice and to $4L^2/a^2$ for the bcc lattice.

The coarse-grained version of Eq. (27) analogous to Eq. (19) is

$$N_i^c(t+\delta t) = N_i^c(t) + \delta N_{\mathrm{di}}\{c_j\} + \delta N_{fi}^c. \tag{30}$$

Here, the local concentration c_j in the diffusional term δN_{di} is $N_j^c(t)/N_L$, while the last term is the sum of coarse-grained fluctuative transfers δN_{fs}^c across all facets s: $\delta N_{fi}^c=\Sigma_s\delta N_{fs}^c$. This transfer δN_{fs}^c is obtained from the full stochastic distribution δN_{fs} determined by Eqs. (28) and (29) by a filtration of noise procedure, that is, by introducing a proper cutoff factor $F_c(\mathbf{k})$ in the Fourier component $\delta N_{f\alpha}(\mathbf{k})$ of the full function $\delta N_{fs} = \delta N_{f\alpha}(\mathbf{R}_{s\alpha})$ where $\mathbf{R}_{s\alpha}$ stands for the center of facet s normal to the main crystal axis α,

$$\delta N^c_{f\alpha}(\mathbf{R}_{s\alpha}) = \sum_{\mathbf{k}} \exp(-i\mathbf{k}\mathbf{R}_{s\alpha})\delta N_{f\alpha}(\mathbf{k})F_c(\mathbf{k}),$$

$$\delta N_{f\alpha}(\mathbf{k}) = \frac{1}{N_{\text{tot}}}\sum_{\mathbf{R}_{s\alpha}} \exp(i\mathbf{k}\mathbf{R}_{s\alpha})\delta N_{f\alpha}(\mathbf{R}_{s\alpha}), \qquad (31)$$

and N_{tot} is the total number of L cells. The cutoff factor $F_c(\mathbf{k})$ is taken in a Gaussian-type form characterized by the cutoff parameter g_L,

$$F_c(\mathbf{k}) = \exp\left[-2g_L^2\sum_{\alpha} \sin^2(k_\alpha L/2)\right]. \qquad (32)$$

where we took into account that the facet centers $\mathbf{R}_{s\alpha}$ at each orientation α form a simple cubic lattice. For the large $g_L^2 \gg 1$ used below, the cutoff function [Eq. (32)] is effectively reduced to a Gaussian $\exp(-k^2l^2/2)$ with the cutoff length $l = Lg_L$. Note that the g_L value in Eq. (32) is related to the quantity g in Eq. (24) as $g_L = ga/L$. Therefore, at $L=2a$, the g_c values presented in the first column of Table II correspond to the values $g_L=10-13$, while at $L=1.5a$, they correspond to $g_L=13-17$.

Equations (19) and (30) and Table II provide a basis for the stochastic statistical description of evolution of microstructure. In what follows, we employ this approach to consider some principal problems in the phase separation kinetics.

VI. MORPHOLOGICAL TRANSITION BETWEEN THE NUCLEATION-GROWTH AND THE SPINODAL DECOMPOSITION EVOLUTION TYPES

A. Theoretical and experimental studies of the transition nucleation and growth–spinodal decomposition

As mentioned in Sec. I, the problem of understanding the morphological transition NG-SD is one of the challenges in the phase transformation theory. This problem was discussed in a number of theoretical and experimental studies,[1,2,24,25] but there seems to be little correlation between the theoretical and the experimental results. In the series of papers reviewed in Ref. 1, Binder and co-workers argued that one cannot expect any clear-cut changes in the phase separation kinetics under crossing the spinodal curve in the c,T plane and, thus, the NG-SD transition should be typically diffuse. These authors also suggested that the spinodal curve, "being a mean-field-based notion," can be manifested only in systems with the large interaction range r_0 for which the MFA is valid and, thus, with increasing r_0, the NG-SD transition should become more sharp. At the same time, in the available experiments,[24–26] the temperature or the concentration intervals for the NG-SD morphological transition, ΔT or Δc, were found to be rather narrow, $\Delta T/T, \Delta c \lesssim 10^{-2}$, while the systems studied in these experiments are supposed to have not too extended interactions.[25,27]

Below, we use simulations based on our stochastic kinetic equations (19) and (30) to elucidate the NG-SD transition problem. All simulations described in this paper include a "preannealing" stage at the temperature $T'_{\text{ann}}=1.2$ for the interval $\Delta t'_{\text{ann}}=0.5$, where t' is the reduced time in the natural time units defined as $t'=t\gamma_{nn}10^{-3}$. The time step δt entering Eq. (19) or (27) was varied between $0.025\gamma_{nn}^{-1}$ and $0.25\gamma_{nn}^{-1}$, most often between $0.05\gamma_{nn}^{-1}$ and $0.1\gamma_{nn}^{-1}$, depending on the alloy system considered and on the stage of its phase separation.

B. Phase separation in quasi-two-dimensional systems near the critical point: Experiments and modeling

Experimentally, the NG-SD morphological transition was most thoroughly studied by Tanaka *et al.*[25,26] for some highly viscous liquid mixture of styrene oligomer (OS) and ϵ-caprolactan oligomer. The critical temperature was $T_c = 156\ ^\circ\text{C}$ and the critical composition was 80 wt % OS, while the binodal temperature for the (35/65) composition used in these studies was 150 °C; thus, the measurements were made near the critical point. The mixture was sandwiched by two glass plates whose gap was several micrometers. This gap seems to be of the order or less than the size of smallest precipitates seen in these experiments; thus, the system can be viewed as a quasi-two-dimensional one.

To theoretically study features of phase separation in quasi-2D systems near T_c, we made simulations for fcc alloys by using the continuous version of SKE [Eqs. (27)–(32)]. As discussed in Sec. II and below, near T_c, this continuous approximation is valid. We consider the concentration $c=0.4$ and the reduced temperatures $T'=T/T_c$ between $T'=0.98$ and $T'=0.94$, while the MFA spinodal temperature at this c is $T'_s=0.96$. These c and T' values are close to those used in experiments;[25] thus, our results can be directly compared to these experiments.

As mentioned in Sec. II, in the continuous MFA used, the interaction model is fully characterized by the reduced interaction radius $r'_0=r_0/a$. We employ three such models: the nearest-neighbor interaction model with $r'_0=2^{-1/2}=0.707$, the

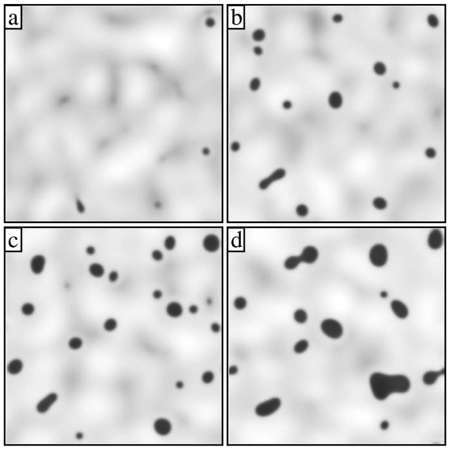

FIG. 5. Temporal evolution of $n(\mathbf{R})$ described by the continuous equations [Eqs. (27)–(31) and (30)] for the fcc alloy model with $r'_0=1$ at $L=2a$, $V_s=(256^2\times 1)L^3$, $g_c=l_c/a=26$, $c=0.4$, $T'=0.98$, and the following $t'=t\gamma_{nn}/1000$: (a) 20, (b) 50, (c) 100, and (d) 250. The gray level linearly varies with $c(\mathbf{R})$ between $n_{\text{min}}=0.3$ and $n_{\text{max}}=0.65$ from completely bright to completely dark.

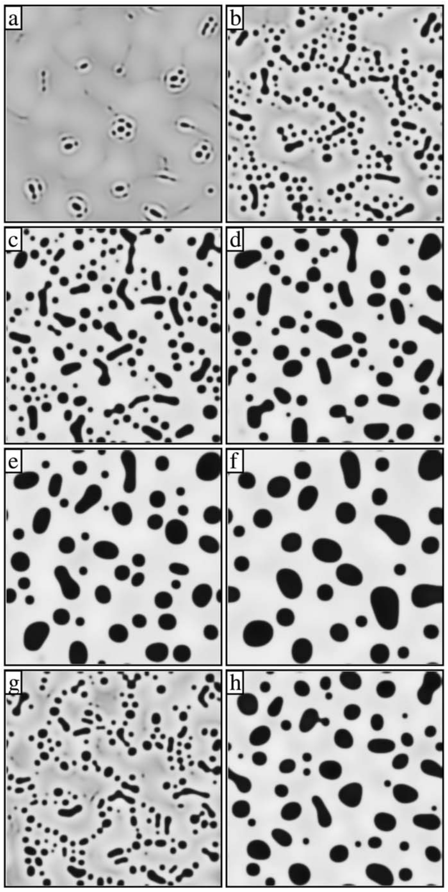

FIG. 6. Frames (a)–(f): same as in Fig. 5 but at $T'=0.94$, $n_{\min}=0.25$, $n_{\max}=0.75$, and the following t': (a) 5, (b) 10, (c) 20, (d) 50, (e) 100, and (f) 200. Frames (g) and (h): same as in frames (a)–(f) but at $g_c=20$ and the following t': (g) 7 and (h) 70.

intermediate interaction range model with $r_0'=1$, and the extended interaction model with $r_0'=2$. At $r_0'=1$ and $r_0'=2$, we use the mesh size $L=2a$, and at $r_0'=0.707$, we use the lesser value $L=1.5a$. The latter is chosen as at $r_0'=0.707$ and at the lowest temperature of these simulations, $T'=0.94$, the second inequality [Eq. (12)] at $L=2a$ is significantly violated. It is manifested in a spurious squarelike anisotropy of precipitates observed in the simulations with $L=2a$, while at $L=1.5a$, these spurious effects are absent.

We made quasi-2D simulations on the fcc lattice with the simulation volume $V_s=(256^2\times 1)L^3$ and the periodic boundary conditions in all three dimensions (such boundary conditions were used in all simulations of this work). Some results of these simulations are shown in Figs. 5–10.

Let us first discuss Figs. 5 and 6 showing the evolution of the NG and the SD type, respectively. The patterns presented in these figures reveal all main features of these two types of evolution illustrated by Figs. 2 and 3 in the paper by Tanaka *et al.*[25] Discussing their observations, these authors wrote "in NG the nuclei… are born and grow almost independently. The density of droplets in NG is much lower than that in SD. In SD, the spatial concentration fluctuations grow in both amplitude and size and form droplets, being first gray, become darker with time, and become larger and larger mainly by coalescence mechanism." All these features are seen in Figs. 5 and 6.

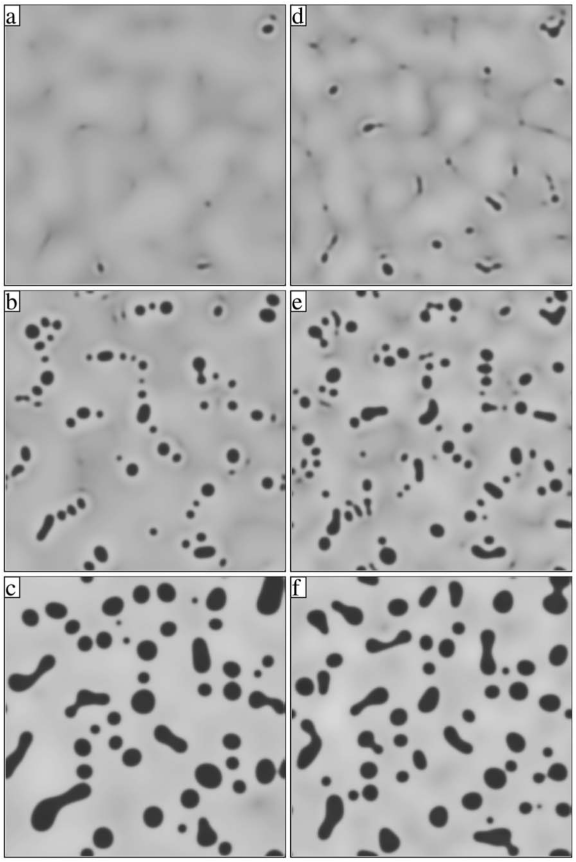

FIG. 7. Frames (a)–(c) (left column): same as in Fig. 5 but at $T'=0.96$, $g_c=26$, and the following t': (a) 7, (b) 14, and (c) 43. Frames (d)–(f) (right column): same as in frames (a)–(c) but at $g_c=20$ and the following t': (d) 5, (e) 10, and (f) 30.

The simulations also reveal a number of other microstructural features. In particular, for the NG-type evolution in Fig. 5, (i) some rare coalescence events are present as well, (ii) the precipitate shape is often nonspherical, and (iii) a concentration-depleted bright "halo" is typically adjacent to

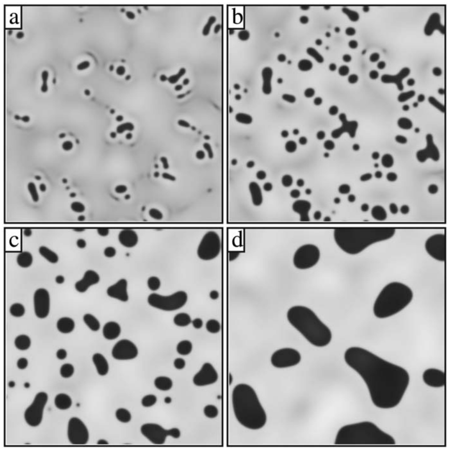

FIG. 8. Same as in Fig. 5 but at $r_0'=0.707$, $T'=0.96$, $L=1.5a$, $g_c=19$, and the following t': (a) 5, (b) 10, (c) 30, and (d) 500.

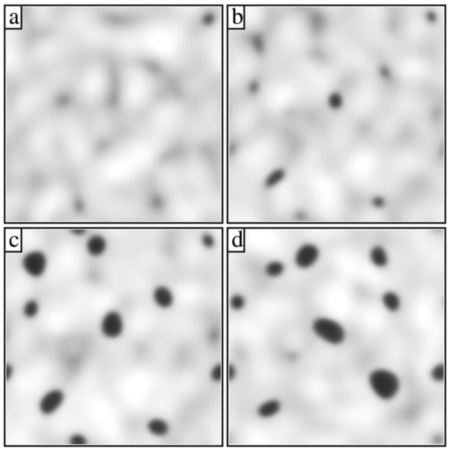

FIG. 9. Same as in Fig. 5 but at $r_0'=2$, $g_c=24$, $T'=0.98$, and the following t': (a) 20, (b) 50, (c) 100, and (d) 250.

the precipitates. For the SD-type evolution in Fig. 6, we observe the following: (i) peculiar initial "roelike" arrays of droplets which later often coalesce forming elongated tonguelike structures and (ii) many coalescence events via a "bridge" mechanism noted in Refs. 15 and 22, when the diffusion fluxes first connect the adjacent precipitates by a thin gray "bridge" that later starts to sharply grow and thicken with the formation of a pearlike or a dumbbell-like precipitate. All of that is seen in the experiments in Refs. 25 and 26.

In our simulation, for the transition region between NG and SD, in particular, for $c=0.4$, $T'=0.96$ just at the spinodal curve, we obtain a "mixed" type of evolution: first, an NG-type pattern of a small number of wrong-shaped droplets, which later form roelike and tongue-like structures characteristic of SD (see Fig. 7). It seems to agree with the observations described in Ref. 25.

Let us comment on the smallness of the temperature width for the NG-SD transition illustrated by Figs. 5 and 6: $\Delta T' \simeq 0.04 \ll 1$. It can be explained by the significant difference in the reduced supersaturation parameter for the alloy states c,T considered. This parameter characterizes a tendency to the NG- or the SD-type evolution and can be defined as[28]

$$s(c,T)=[c-c_b(T)]/[c_b(T)-c_s(T)], \tag{33}$$

where $c_b(T)$ and $c_s(T)$ are the concentrations at the binodal and the spinodal curves, respectively. For the two states considered, this parameter takes quite different values, $s_1=0.42$ and $s_2=1.27$, even though the temperature difference $\Delta T'$ is small. It is because the (c,T) states considered are positioned near the critical point where both the binodal and the spinodal curves are very flat. It can be still more so for experiments,[25] where the curves $T_b(c)$ and $T_s(c)$ seem to be still flatter than in our MFA model. It can explain a rather small value of the NG-SD transition width, $\Delta T' \simeq 0.015$, found in Ref. 25.

Let us still make a methodical comment about the applicability of the continuous approximation [Eqs. (27)–(32)] for the simulations described above, in particular, at our lowest temperature $T'=0.94$. To check this point, we repeated some of these simulations by using the general discrete lattice approach [Eqs. (19)–(24)] and the fcc-3 interaction model defined in Table I. For this model, the reduced interaction radius r_0' is unity, just as for the model used in the simulations illustrated by Figs. 7–9. The discrete and the continuous approaches were found to yield very similar results seeming to be statistically identical. It is illustrated in Fig. 2 by the results for $J_m(g)$ at $r_0'=1$, $c=0.4$, and $T'=0.94$, which are shown by crosses for the discrete approach and by open circles for the continuous approach. In the physically interesting region $g \gtrsim g_c = 20-26$ where the above-discussed local equilibrium takes place, these results do virtually coincide with each other. Thus, the continuous approximation can be safely used for the above-described simulations at T near T_c.

C. Dependence of the type of microstructural evolution on the interaction range

To study the influence of varying the interaction range r_0 on the microstructural evolution, in particular, to check the considerations about the "sharpening" of the NG-SD transition with increasing r_0 mentioned above,[1] we made simulations of phase separation similar to those described above but for several other models with the different r_0 values. Some results of these simulations are shown in Fig. 8 for the short-range-interaction model with $r_0'=0.707$, and in Figs. 9 and 10 for the extended interaction model with $r_0'=2$. These figures can be compared to Figs. 7–9, which illustrate the evolution of systems with the "intermediate" $r_0'=1$. As the real physical parameters of an alloy, such as the number of atoms within the interaction range, N_{int}, or the critical embryo volume V_c, depend on the r_0 value rather sharply, $N_{\text{int}}, V_c \propto r_0^3$, the three times change in r_0 can enable us to see how the evolution type varies with the interaction range.

The comparison of Figs. 5–10 shows that both the morphological and the kinetic characteristics of evolution strongly depend on the interaction range. With increasing r_0, all characteristic lengths in the microstructures, in particular, sizes of smallest precipitates, rise approximately linearly in r_0. The evolution rate notably decreases, particularly at very

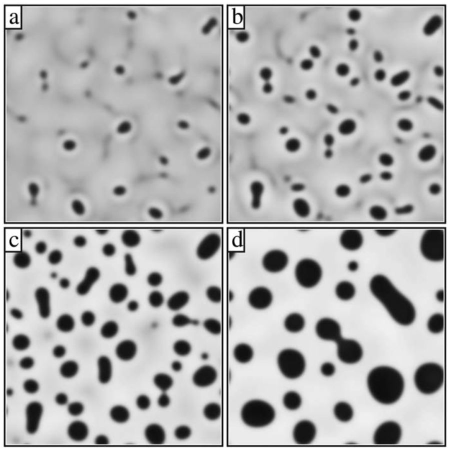

FIG. 10. Same as in Fig. 9 but at $T'=0.94$ and the following t': (a) 7, (b) 10, (c) 20, and (d) 200.

first stages of phase separation. The precipitate shape becomes more regular and more spherical, while the formation of roelike structures at SD mentioned above is suppressed. All these effects can be qualitatively explained by an increase of the interfacial energy σ with increasing r_0, which is discussed below in Sec. VII.

At the same time, we see no hints of "sharpening" or "narrowing" the morphological transition NG-SD with increasing r_0. On the contrary, the comparison of Figs. 5 and 6 to Figs. 9 and 10 seems to imply that at larger r_0, this transition becomes more smeared and more wide. In particular, both morphological and temporal characteristics of microstructural evolution at two temperatures considered, $T'=0.98$ and $T'=0.94$, for the intermediate-interaction-range model with $r_0'=1$ seem to differ with each other more strongly than those for the extended-interaction-range model with $r_0'=2$.

The disagreement with the previous considerations[1] can be due to that these considerations were mainly based on the thermodynamic arguments, while the strong dependence of the kinetic factors on the interaction range was disregarded. Our results show that this dependence can be actually more sharp and more important for the microstructural evolution.

D. Morphological transition nucleation and growth–spinodal decomposition at intermediate temperatures

Studies of quasi-2D phase separation at T near T_c described in Sec. VI B enable us to suggest that the type of the microstructural evolution under phase separation is mainly determined by the reduced supersaturation parameter s value defined by Eq. (33). Values $s \lesssim s_1 \simeq 0.5$ seem to correspond to NG, and values $s \gtrsim s_2 \simeq 1.2$ to SD, while varying s between s_1 and s_2 leads to the gradual transition between these two types of evolution.

To check this point in more detail, in this section, we consider phase separation in both 2D and 3D systems in a more broad temperature interval, $0.7 \lesssim T' \lesssim 0.9$, for brevity to be called "the intermediate temperatures." At the lower temperatures, $T' \lesssim 0.5$, the crystalline anisotropy effects become important, and these effects are discussed in the next section.

Outside the critical region, the interphase boundary width $w_{\rm ipb}$ and the lattice constant a generally have the same order of magnitude, and the second inequality [Eq. (12)] does not hold. Thus, the continuous approximation [Eqs. (27)–(32)] becomes inapplicable, and the general discrete lattice approach [Eqs. (19)–(24)] should be used.

To study the influence of various factors on the phase separation kinetics at intermediate T, we made simulations based on the SKE [Eqs. (19)–(24)] for a number of different concentrations c, temperatures T, and the models of interactions v_{ij}, keeping the reduced supersaturation s close to either of the two above-mentioned values, s_1 or s_2. The simulations seem to confirm that the evolution type is mainly determined by the value of s, but at the given s, the kinetic characteristics and the details of microstructure can strongly vary with c, T, and v_{ij}.

To illustrate these points, in Figs. 11–14, we present some results of such simulations made at the concentrations and temperatures given in Table III and shown in Fig. 1 as (c,T) points A, B, C, and D. These four points form an asymmetric "cross" in the (c,T) plane near the spinodal point S, and points A and D correspond to the NG-type value $s\simeq 0.47$, while points B and C correspond to the SD-type value $s\simeq 1.18$.

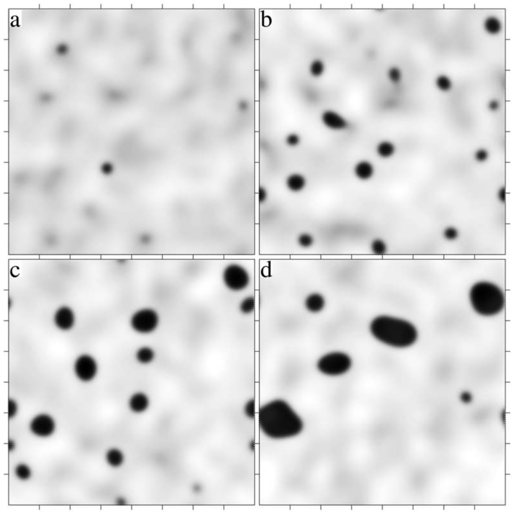

FIG. 11. Temporal evolution of n_i described by the discrete lattice equations [Eqs. (19)–(24)] for the bcc-3 model described in the text at $V_s=(128^2\times 1)a^3$, $g_c=5$, $c=0.25$, $T'=0.86$, $s=0.47$, $n_{\rm min}=0.15$, $n_{\rm max}=0.85$, and the following t': (a) 0.3, (b) 1, (c) 2, and (d) 10.

Figures 11 and 12 correspond to quasi-2D simulations similar to those discussed in Sec. VI B. Thus, these figures enable us to compare the evolution at intermediate T to the evolution near T_c shown in Figs. 5 and 6. Figures 13 and 14 correspond to the 3D simulation, but for simplicity, they show only one crystal plane. We made also some checking runs by using the larger simulation volume, $V_s=(64^2\times 16)a^3$, and the results were found to be very similar to

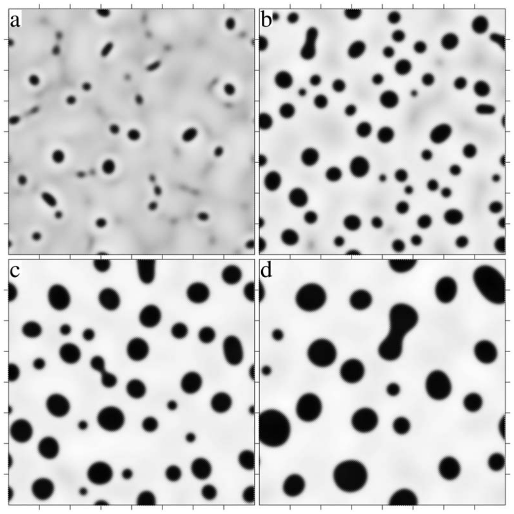

FIG. 12. Same as in Fig. 11 but at $c=0.25$, $T'=0.7$, $s=1.17$, $n_{\rm min}=0.05$, $n_{\rm max}=0.95$, and the following t': (a) 0.08, (b) 0.2, (c) 1, and (d) 4.

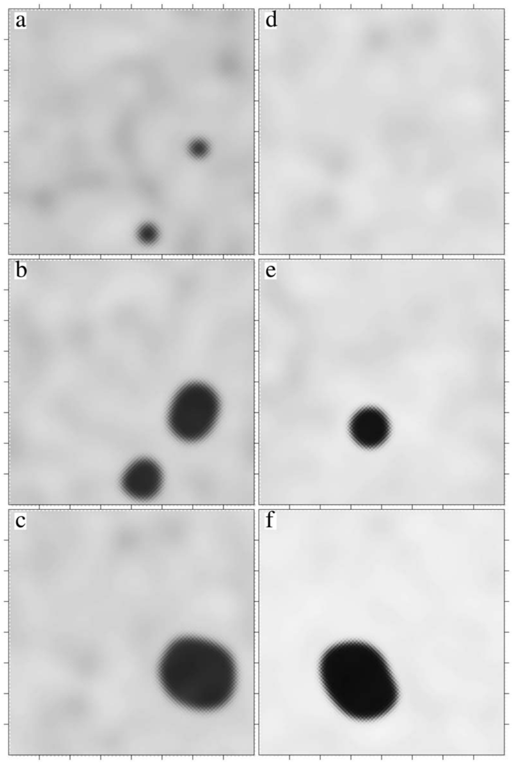

FIG. 13. Same as in Fig. 11 but for 3D simulations using the bcc-1 model at $V_s=(64^2\times 8)a^3$, $g_c=3$, and shown for the crystal plane $z=0$. Frames (a)–(c) correspond to $c=0.25$, $T'=0.86$, $s=0.47$, $n_{\min}=0.15$, $n_{\max}=0.85$, and the following t': (a) 2, (b) 5, and (c) 10. Frames (d)–(f) correspond to $c=0.175$, $T'=0.75$, $s=0.46$, $n_{\min}=0.05$, $n_{\max}=0.95$, and the following t': (d) 20, (e) 22, and (f) 30.

those shown in Figs. 13 and 14. Therefore, the "finite-size" effects in these simulations seem to be unessential, and Figs. 13 and 14 can represent a true 3D microstructural evolution.

Let us discuss the results presented in Figs. 11–14. Comparing quasi-2D microstructures at intermediate T shown in Figs. 11 and 12 to those near T_c shown in Figs. 5 and 6, we first note that the scale of frames in Figs. 5 and 6 (at the given lattice constant a) is by four times larger than that in Figs. 11 and 12. Therefore, all microstructural lengths characteristic of phase separation, such as the sizes of initial ("critical") precipitates at NG or the wavelengths of unstable concentration waves at SD,[9,22] in the critical region $T\simeq T_c$ much exceed those at intermediate T. It illustrates a sharp increase of all these lengths with approaching T_c, which was repeatedly mentioned above.

Let us also note that the analogous quasi-2D microstructures simulated for model bcc-1 (not shown here to save space) are rather similar to those for model bcc-3 presented in Figs. 11 and 12. It agrees with the relatively small difference in the interaction range between these two models: $r_0'(\text{bcc-3})\simeq 1.2r_0'(\text{bcc-1})$.

Discussing 3D simulations of the NG-type evolution illustrated in Fig. 13, we first note that in spite of the general similarity of this evolution for c,T point A and point D shown in frames 13(a)–13(c) and (13d)–(13f), respectively, the quantitative characteristics of nucleation for these two points notably differ. The size of initial precipitates for point D, $R_c(\text{D})$, seems to significantly exceed that for point A, $R_c(\text{A})$, while the reduced incubation time (the time needed for the formation of first precipitates[3]) for point D, $t'_{\text{inc}}(\text{D})$, appears to exceed the analogous time $t'_{\text{inc}}(\text{A})$ by an order of magnitude. At the same time, for points B and C with the SD-type evolution, both space and time characteristics of microstructures shown in Fig. 14 seem to be very similar.

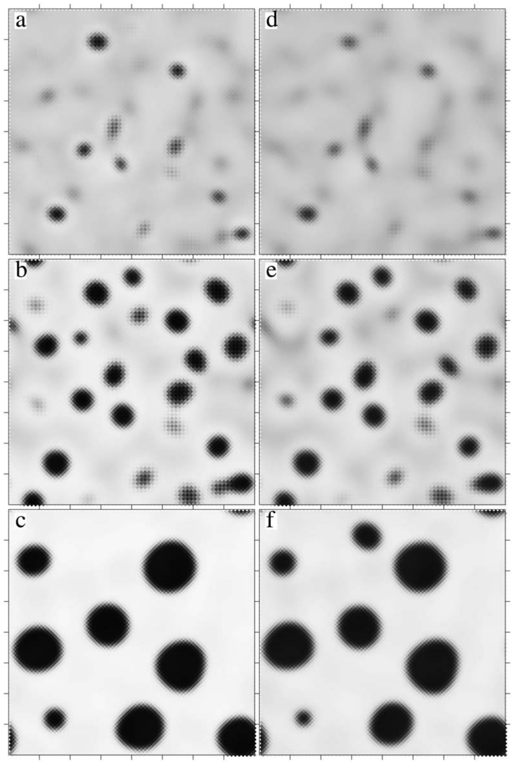

FIG. 14. Same as in Fig. 13 but at $n_{\min}=0.05$, $n_{\max}=0.95$. Frames (a)–(c) correspond to $c=0.25$, $T'=0.7$, $s=1.17$, and the following t': (a) 0.05, (b) 0.1, and (c) 5. Frames (d)–(f) correspond to $c=0.275$, $T'=0.75$, $s=1.18$, and the following t': (d) 0.05, (e) 0.1, and (f) 5.

In spite of all the differences mentioned above, the results presented in Figs. 5, 6, and 11–14 seem to strongly support the above-mentioned conjecture that the type of microstructural evolution under phase separation, both near T_c and at intermediate T, is mainly determined by the reduced supersaturation s value. It is supported, in particular, by comparing to each other Figs. 5, 11, and 13 for the NG-type evolution and Figs. 6, 12, and 14 for the SD-type evolution. For each

TABLE III. Values of thermodynamic parameters used in the simulations of phase separation at intermediate temperatures.

Point in Fig. 1	c,T'	s
S	0.25, 0.75	1
A	0.25, 0.86	0.47
B	0.275, 0.75	1.18
C	0.25, 0.7	1.17
D	0.175, 0.75	0.46

of these two evolution types, the microstructures shown in the three figures reveal a striking similarity in all main features, even though the alloy models used and their thermodynamic and kinetic characteristics are sometimes rather different.

Once the evolution type is mainly determined by the reduced supersaturation s, the concentration or the temperature width for the NG-SD transition, Δc or $\Delta T'$, should significantly vary under variations of c or T' along the spinodal curve. In particular, in vicinity of the spinodal point S considered in this section, these widths are estimated as $\Delta c \simeq 0.1$ and $\Delta T' \simeq 0.16$, while in vicinity of the spinodal point $(c_s, T'_s) = (0.4, 0.96)$ discussed in Sec. VI B, the temperature width is much smaller: $\Delta T' \simeq 0.04$.

VII. MORPHOLOGY OF PRECIPITATES AND KINETIC FEATURES OF PRECIPITATION AT LOW TEMPERATURES

By discussing manifestations of anisotropy in morphology of precipitates, we first note that here we do not consider the anisotropic effects related to the long-ranged elastic interaction induced by the precipitate-matrix lattice misfit. At early stages of phase separation being studied in this work, such effects are typically small due to the small size of precipitates,[10,15] the more so if the misfit is small which is the case, in particular, for the Al-Ag and Fe-Cu alloys discussed below. Here, we consider the anisotropic effects related to the short-ranged "chemical" interaction, which can be manifested at sufficiently low $T' \lesssim 0.5$. These effects were discussed in several experimental[29] and theoretical[4] studies. Below, we consider them by using the SKE [Eqs. (19)–(24)].

Let us first discuss the way of visualization of our results for the 3D patterns. For the 2D patterns, each lattice site i in Figs. 11–14 was represented as an elementary square with the area $a^2/2$ for the bcc lattice (or $a^2/4$ for the fcc lattice[15]). The gray level for each square was linearly varied with the site occupation n_i defined by Eqs. (19)–(24) between some minimal and maximum values, $n_{\min}$ and $n_{\max}$, from completely bright to completely dark. For the 3D patterns, it is more convenient to represent lattice sites as nonoverlapping spheres. For each sphere, the gray level again linearly varies with n_i between some $n_{\min}$ and $n_{\max}$, but to make the figures transparent, it is convenient to omit all "almost empty" sites with $n_i \leqslant n_{\min}$. Therefore, the proper choice of the cutoff value $n_{\min}$ is here important for the adequate representation of evolution, but this choice can be optimized for each particular system. In Figs. 15–19 and 21 discussed below, $n_{\min}$ is chosen to slightly exceed the mean concentration c.

By considering morphology of precipitates, we first discuss the influence of varying the interfacial energy scale on this morphology. A possible importance of such influence was mentioned by Ernst and Haasen[29] in their study of phase separation in the disordered fcc Al-Ag alloys by the high resolution electron microscopy methods. After annealing at $T' \simeq 0.5$, the precipitates were clearly facetted, and straight interfaces parallel to {100} and {111} planes were often observed. At the same time, for the most of phase-separating alloys, anisotropic effects at such relatively high temperatures are not revealed. Ernst and Haasen noted that "this observation confirms the relatively small value of the interfacial energy" for these alloys (found from other measurements) but did not discuss this point. Below, we consider the relation between the scale of the interfacial energy and the degree of anisotropy of precipitates in more detail.

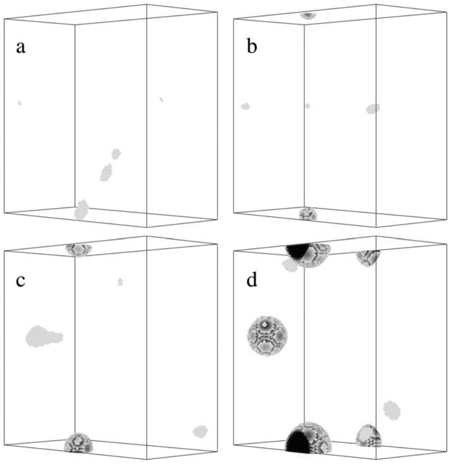

FIG. 15. Temporal evolution of n_i according to Eqs. (19)–(24) shown in the 3D representation described in Sec. VII for the fcc-1 model at $V_s = (64^2 \times 32)a^3$, $g_c = 3$, $n_{\min} = 0.147$, $n_{\max} = 1$, $c = 0.11$, $T' = 0.5$, $s = 0.71$, and the following t': (a) 0.2, (b) 0.25, (c) 0.3, and (d) 0.5.

To study this problem, we made the SKE-based simulations of phase separation at $T' = 0.5$ for several alloy models with the different scale of the interfacial energy. The concentration value was chosen so that the volume fraction of pre-

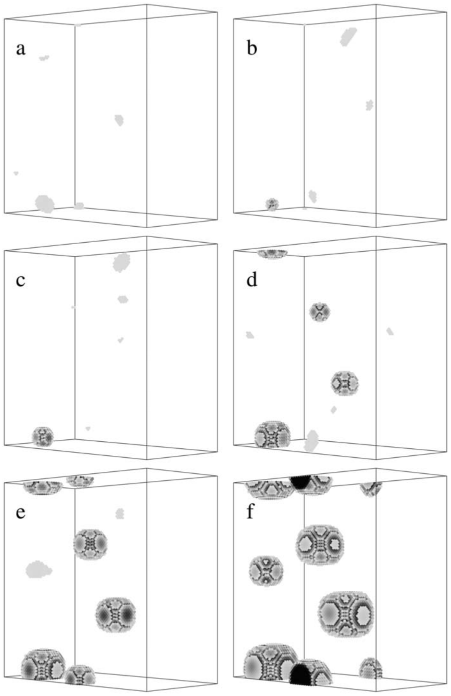

FIG. 16. Same as in Fig. 15 but for the fcc-3a model described in the text at the following t': (a) 0.05, (b) 0.07, (c) 0.1, (d) 0.2, (e) 0.3, and (f) 0.5.

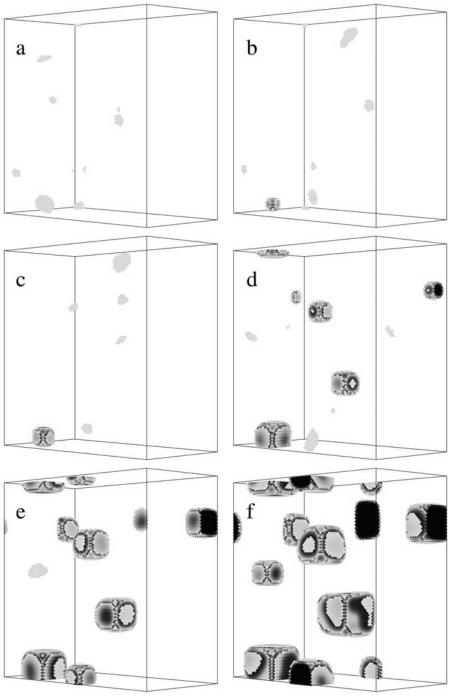

FIG. 17. Same as in Fig. 15 but for the fcc-3b model described in the text at the following t': (a) 0.05, (b) 0.07, (c) 0.1, (d) 0.2, (e) 0.3, and (f) 0.5.

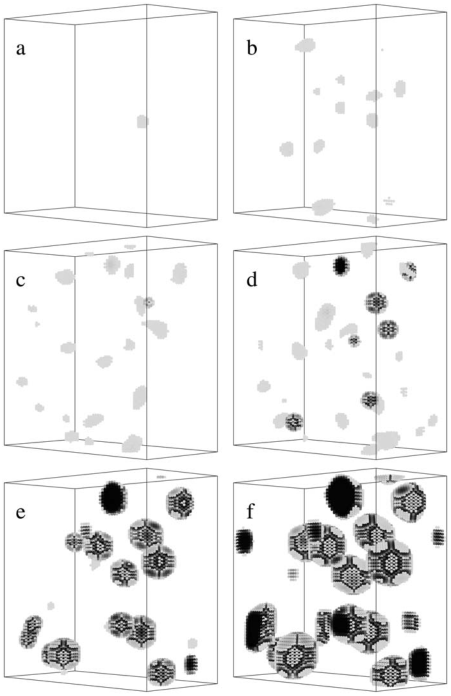

FIG. 19. Same as in Fig. 15 but for the bcc-3a model described in the text at the following t': (a) 0.01, (b) 0.02, (c) 0.06, (d) 0.1, (e) 0.2, and (f) 0.5.

cipitates was similar to that observed in experiments:[29] $c=0.11$. It corresponds to the reduced supersaturation $s=0.71$, that is, to the NG region in the (c,T) plane not far from the spinodal curve. The surface energy σ was estimated in the continuous approximation by using the Ginzburg–Landau (or Cahn–Hilliard[21]) free energy functional F,[12]

$$F=\frac{1}{v_a}\int d^3R[g_{cc}(\nabla c)^2+f(c)]. \tag{34}$$

Here, v_a is atomic volume, $c=c(\mathbf{R})$ is the local concentration, and $f(c)$ is the free energy per site, which in the MFA used has the form

$$f(c)=T[c\ln c+(1-c)\ln(1-c)]+V_0c^2/2, \tag{35}$$

where $V_0=\Sigma_j v_{ij}$ is the MFA interaction parameter. Microscopic expressions for the coefficient g_{cc} in Eq. (34) were discussed in Ref. 12. In the MFA used, this coefficient is some constant proportional to the mean interaction radius squared r_0^2 that enters Eq. (10). The interfacial energy $\sigma=\sigma(T)$ for the functional [Eq. (34)] is given by the following expression:[12,21]

$$\sigma(T)=\frac{1}{v_a}\int_{c_{01}}^{c_{02}}dc\{g_{cc}[\Omega(c)-\Omega_0]\}^{1/2}. \tag{36}$$

Here, c_{01} and c_{02} are the equilibrium concentrations for the two phases under consideration, $\Omega(c)$ is $f(c)-c\mu_0$, the chemical potential μ_0 and Ω_0 are the values of $\mu(c)=\partial f/\partial c$ and $\Omega(c)$, respectively, at $c=c_{01}$ or $c=c_{02}$, while the relations $\mu(c_{01})=\mu(c_{02})$ and $\Omega(c_{01})=\Omega(c_{02})$ are the phase equilibrium conditions.

Formally, the Ginzburg–Landau expression [Eq. (36)] is valid only at high temperatures near T_c when the interphase boundary width much exceeds the interatomic distance and the interfacial energy is isotropic.[12] However, this expression can also be used to estimate the average surface energy at lower T, in particular, at $T'\sim 0.5$ under consideration.

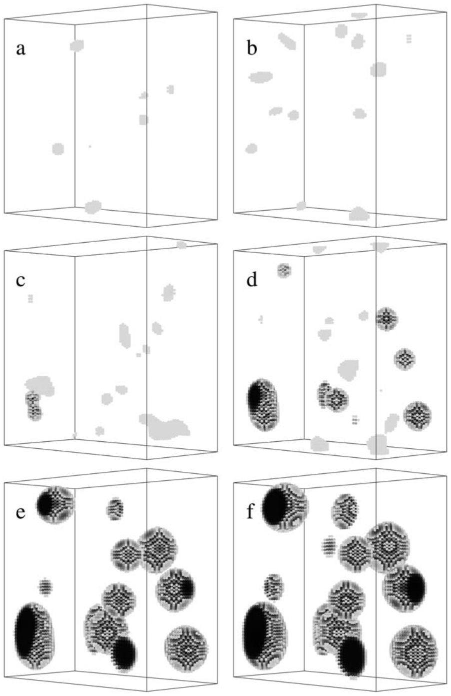

FIG. 18. Same as in Fig. 15 but for the bcc-1 model at the following t': (a) 0.05, (b) 0.07, (c) 0.18, (d) 0.3, (e) 0.5, and (f) 1.

In our simulations, we employed three alloy models: the nearest-neighbor-interaction model fcc-1 and the two three-neighbor-interaction models, fcc-3a and fcc-3b, described in Table I. For the fcc-1 model, the reduced surface energy $\sigma' = \sigma a^2/T_c$ with σ given by Eq. (36) at $T'=0.5$ is $\sigma'=0.91$. For the two other models, the interaction constants are chosen so that the reduced surface energies at $T'=0.5$ take the following values:

$$\sigma'_{\text{fcc-3a}} = 0.7, \quad \sigma'_{\text{fcc-3b}} = 0.5. \tag{37}$$

Thus, the interfacial energies for these three models differ notably, and simulations of phase separation for these models enable us to follow the influence of varying the interfacial energy on the microstructural evolution and morphology of precipitates.

In Figs. 15–17, we present some results of these simulations. First, we see that for the fcc-1 model for which the interfacial energy has the "normal" scale $\sigma' \sim 1$, the shape of precipitates at $T'=0.5$ is almost spherical, and their anisotropy is weak. For the fcc-3a model with the lower σ', we observe, first, the smaller size of new-born precipitates and some acceleration of nucleation with respect to the fcc-1 model. It qualitatively agrees with the decrease of both the critical size and of the nucleation barrier under lowering the surface energy, which are the well-known conclusions of the classical nucleation theory.[3] Second, we note a much more pronounced faceting of precipitates in {100} planes. Finally, for the fcc-3b model with the lowest σ', the nucleation rate seems to still more increase, the precipitate shape is typically highly anisotropic, and, in addition to that, at later stages of evolution some precipitates have a number of wrong-shaped facets. The latter again agrees with the experimental observations.[29]

To elucidate the influence of the crystal lattice type on the above-mentioned effects, we also made similar simulations for the bcc alloys with the same values of thermodynamic parameters: $c=0.11$, $T'=0.5$, and $s=0.71$. We used two models: the nearest-neighbor-interaction model bcc-1 and the three-neighbor-interaction model bcc-3a described in Table I. The reduced average surface energies (estimated by the above-described method) for these models are

$$\sigma'_{\text{bcc-1}} = 0.56, \quad \sigma'_{\text{bcc-3a}} = 0.3, \tag{38}$$

differing by about twice.

Some results of these simulations are shown in Figs. 18 and 19. For the short-range-interaction model bcc-1, the precipitates again are almost spherical, though the fusion processes, such as that seen in the left lower corner of frames (c)–(e), can lead to an elongation of some of them. For the bcc-3a model with the lower σ', we again observe the smaller size of new-born precipitates and the higher nucleation rate, as well as much more pronounced faceting in the {110} planes.

Therefore, the effects of variations of interfacial energy on the kinetics of phase separation in the fcc and the bcc alloys turn out to be similar, and the manifestations of these effects in morphology of precipitates agree well with the observations by Ernst and Haasen.[29]

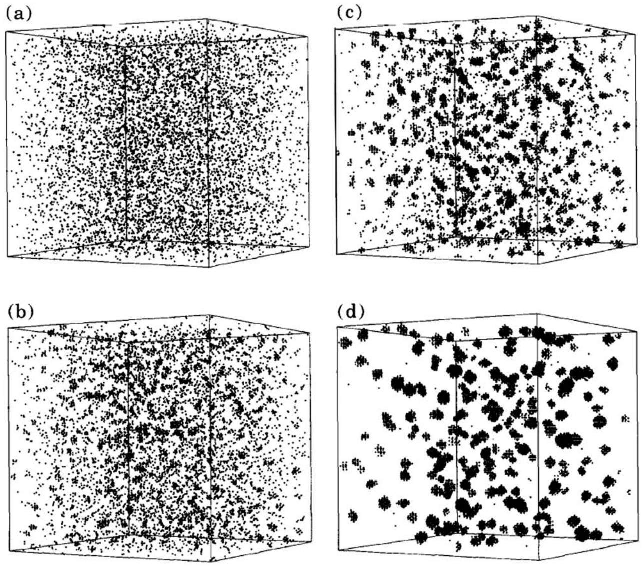

FIG. 20. Evolution of precipitate microstructure for the bcc-1 model of Fe-Cu alloy with the vacancy-mediated atomic exchange according to the Monte Carlo simulation made in Ref. 4 at $V_s = 64^3a^3$, $c=0.0134$, $T'=0.182$, and the following times t (in 10^7 s): (a) 0, (b) 5.8, (c) 24, and (d) 270. Each dot represents a copper atom.

Let us now discuss the kinetics of phase separation at low $T' \lesssim 0.2-0.3$. This problem attracts interest, in particular, in connection with the copper precipitation in the dilute iron-copper alloys, which is important for a number of industrial applications.[4,6,7] This problem was thoroughly discussed by Soisson *et al.*,[4] who made detailed Monte Carlo simulations of this process by using the KMCA mentioned in Sec. I. Some results of these simulations are presented in Fig. 20. These results illustrate a number of peculiar features characteristic of precipitation at low temperatures, in particular, (i) a very small size of initial (critical) precipitates that often include 2–5 atoms, (ii) the nonspherical shape of these initial precipitates with nonplanar precipitate-matrix interfaces, and (iii) a strong tendency to the formation of {110} facets at longer precipitation times and other features discussed in Ref. 4.

To study this problem within our stochastic statistical approach (SSA), as well as to compare this approach to the KMCA, we made the SSA-based simulations of phase separation for the alloy model and thermodynamic conditions similar to those considered in Ref. 4. We use the bcc-1 model at $T'=0.18$ within simulation volume $V_s=64^3a^3$, just as Soisson *et al.* did, but consider a bit higher concentration $c=0.03$ that corresponds to the reduced supersaturation $s=0.64$. The results discussed below seem to show that employing this c value can be sufficient to study the problem under consideration. At the same time, at lower $c<0.015$ used in Ref. 4 (which corresponds to the reduced supersaturation $s<0.3$), the incubation time in our simulations becomes too large to observe any precipitation for our typical simulation times $t' \lesssim 10$. Thus, elaboration of methods for the SSA treatments of phase separation at low supersaturations is a separate methodical problem (similar to that encountered in the KMCA treatments[5]).

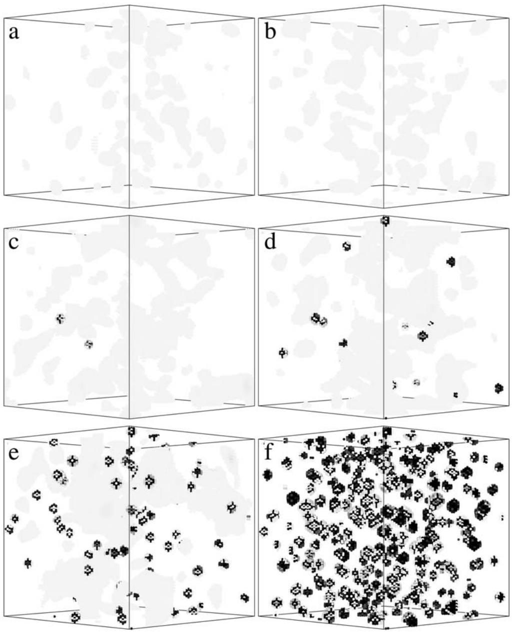

FIG. 21. Same as in Fig. 15 but for the bcc-1 model at $V_s=64^3a^3$, $g_c=3$, $n_{\min}=0.04$, $n_{\max}=1$, $c=0.03$, $T'=0.18$, $s=0.636$, and the following t': (a) 0.01, (b) 0.02, (c) 0.05, (d) 0.1, (e) 0.2, and (f) 0.5.

Some results of our simulation are presented in Fig. 21. Before to compare the SSA and the KMCA results, we note that the two approaches use the different methods of describing the alloy states. In the KMCA, each alloy state at time t is characterized by the positions of all minority (copper) atoms, while in the SSA, the local mean occupations $n_i(t)$ are presented. These $n_i(t)$ correspond to the averaging of site occupations n_i over some locally equilibrated regions. It also implies a temporal averaging for the appropriate time intervals Δt (see Ref. 8, Sec. VII), being much greater than one interatomic exchange time $t_{\mathrm{exc}} \sim \gamma_{nn}^{-1}$ but much less than the characteristic time t_c needed for a significant variation of $n_i(t)$,

$$\gamma_{nn}^{-1} \ll \Delta t \ll t_c. \tag{39}$$

Figures 5–19 and 21 show that the relation $\gamma_{nn} t_c \gg 1$ implied by these inequalities is well satisfied for all evolution processes considered in this paper.

The alloy systems shown in Figs. 20 and 21 also differ in a number of other respects. In addition to the composition difference mentioned above, their critical temperatures differ, too. In the SSA simulation, the T_c value for the bcc-1 model is calculated by using the MFA, while in the KMCA, it is taken from Monte Carlo simulation; it yields $T_c^{\mathrm{KMCA}} = 0.79 T_c^{\mathrm{MFA}}$. The kinetic mechanisms are different, too. The SSA employs the simplified direct-atomic-exchange model, while the KMCA uses a more realistic model of the vacancy-mediated atomic exchange.

In spite of all these differences both in the alloy model and in the way of describing its states, the main features of evolution shown in Figs. 20 and 21 seem to reveal a great similarity, and the SSA description appears to complement the KMCA one in some respects. In particular, frames 21(a) and 21(b) present a visualization of some initial and some more advanced "incubation" stages, respectively, illustrating an increase of the composition fluctuations with time. Frames 21(c) and 21(d) show the first stages of precipitation and seem to approximately correspond to the stage shown in frame 20(b). The microstructure shown in frame 21(e) resembles that presented in frame 20(c), while the microstructure shown in frame 21(f) seems to be similar to that in frame 20(d). The smallest precipitates in frames 21(c) and 21(d) seem to include three to five atoms, in accordance to point (i) mentioned above, and their shape reveals neither sphericity nor the planar interfaces, in accordance to point (ii). At later stages shown in frames 21(e) and 21(f), the growing precipitates demonstrate a pronounced faceting in {110} planes, in agreement with point (iii), as well as with other results by Soisson *et al.*[4] presented in their Fig. 4.

Therefore, the SSA and the KMCA treatments of precipitation at low temperatures discussed above seem to agree with each other in all main respects. At the same time, the comparison of these treatments illustrates some complementary features of these two approaches to the description of evolution of microstructure.

VIII. CONCLUDING REMARKS

Let us summarize the main results of this work. The earlier-suggested generalized Gibbs distribution approach and the QKE for nonequilibrium alloys are generalized to stochastically describe the evolution of microstructure at first stages of phase separation in alloys. The influence of fluctuations of diffusion fluxes (neglected in the QKE) is simulated by using the Langevin-type method similar to that used for the mechanical systems. However, here this method should be supplemented by the "filtration of noise" procedure that physically describes the statistical averaging of site occupations n_i over the appropriate locally equilibrated region with the characteristic size $l_{\mathrm{le}} \sim l_c$. Thus, the theory includes the size l_c as an important kinetic parameter. The resulting stochastic kinetic equation for the mean site occupations $n_i(t)$ generalizes the QKE to the case when the fluctuations of diffusion fluxes mentioned above are important, in particular, when the concentration c and temperature T values are positioned above or near the spinodal curve in the (c,T) plane. For each c,T and the model of interatomic interaction v_{ij}, the size l_c is estimated by using simulations of evolution at different values of this size. The resulting l_c are usually weakly sensitive to the c,T and v_{ij} values, but they sharply rise when the (c,T) point approaches the critical point c_c, T_c.

The methods developed are used to study some general problems in the phase separation kinetics. First, we investigate the microstructural features of both the NG and the SD types of evolution, as well as the morphological transition NG-SD under variations of c and T across the spinodal curve. The results obtained agree well with the available experimental studies of the NG-SD transition.[25,26] Both near the critical point and at intermediate temperatures, $0.7 \lesssim T/T_c \lesssim 0.9$, the microstructural evolution type seems to be mainly determined by the reduced supersaturation parameter s value defined by Eq. (33). We also study the influence of varying the scale of the interfacial energy on the precipitation kinetics at temperatures $T \lesssim 0.5T_c$. When the interfacial energy decreases, the size of new-born precipitates decreases and the nucleation rate increases, which is in qualitative agreement with the ideas of the classical nucleation theory, while anisotropy in the morphology of precipitates sharply rises, which is in agreement with the experimental observations.[29] Finally, we investigate the kinetic features of precipitation at low T for the Fe-Cu alloy model studied earlier by using the KMCA.[4] The results of our SSA for this model agree well with the KMCA results. The comparison also illustrates the complementary character of these two approaches.

Finally, let us make some general remarks about the SSA described in this paper. The main notions used in this approach, such as the macrononequilibrium state consisting of locally equilibrated quasiclosed subsystems, the master equation for the probability distribution, Langevin's method for simulating the influence of fluctuations on evolution, etc., are well known and are described in textbooks and reviews.[8,15,23] Basing on these notions, we attempt to develop an explicit and theoretically consistent approach to study the microstructure of alloys at those concentrations, temperatures, and stages of evolution, at which the role of statistical fluctuations in the phase separation kinetics is crucial. The results described in this paper seem to show that this approach, even in its present form employing just simplest methods and simplest models (such as the mean-field approximation, the direct-atomic-exchange model, etc.), can be rather fruitful and useful for both the understanding and the predictions of many new and nontrivial microstructural phenomena that take place in the course of the phase separation in alloys. Thus, further developments of this approach seem to be promising.

ACKNOWLEDGMENTS

The authors are much indebted to Georges Martin for numerous stimulating discussions and to V. Yu. Dobretsov for the great help at the first stages of this work. The work was supported by the Research Technological Center "Ausferr," Magnitogorsk, by the Russian Foundation for Basic Research (Grant No. 06-02-16476) and by the fund for support of the fundamental projects of RRC "Kurchatov Institute" (Grant No. 11, 2006).

---

[1] K. Binder, in *Materials Science and Technology, Vol. 5: Phase Transformations in Materials*, edited by R. W. Cahn, P. Haasen, and E. J. Kramer (VCH, Weinheim, 1991), Chap. 7.

[2] R. Wagner and R. Kampmann, *Materials Science and Technology: Phase Transformations in Materals* (Ref. 1), Chap. 4.

[3] F. Soisson and G. Martin, Phys. Rev. B **62**, 203 (2000).

[4] F. Soisson, A. Barbu, and G. Martin, Acta Mater. **44**, 3789 (1996).

[5] E. Clouet, M. Nastar, A. Barbu, C. Sigli, and G. Martin, in Solid→Solid *Phase Transformations in Inorganic Materials 2005*, edited by J. M. Howe, D. E. Laughlin, J. K. Lee, U. Dahmen, and W. A. Soffa (TMS, Warrendale, 2005), Vol. 2, pp. 683–704.

[6] M. K. Miller, B. D. Wirth, and G. R. Odette, Mater. Sci. Eng., A **353**, 133 (2003).

[7] D. Isheim, M. S. Gagliano, M. E. Fine, and D. N. Seidman, Acta Mater. **54**, 841 (2006).

[8] L. D. Landau and E. M. Lifshits, *Statistical Physics* (Nauka, Moscow, 1995).

[9] J. W. Cahn, Acta Metall. **9**, 795 (1961).

[10] Y. Wang, D. Banerjee, C. C. Su, and A. G. Khachaturyan, Acta Mater. **46**, 2983 (1998).

[11] W. Guo, Y. Zong, G. Wang, and Y. Wang, Solid→Solid *Phase Transformations in Inorganic Materials 2005*, (Ref. 5), Vol. 2, pp. 757–762.

[12] I. R. Pankratov and V. G. Vaks, Phys. Rev. B **68**, 134208 (2003).

[13] G. Martin, Phys. Rev. B **41**, 2279 (1990).

[14] F. Haider, P. Bellon, and G. Martin, Phys. Rev. B **42**, 8274 (1990).

[15] V. G. Vaks, Phys. Rep. **391**, 157 (2004).

[16] V. G. Vaks, Pis'ma Zh. Eksp. Teor. Fiz. **63**, 447 (1996). [JETP Lett. **63**, 471 (1996)].

[17] K. D. Belashchenko and V. G. Vaks, J. Phys.: Condens. Matter **10**, 1965 (1998).

[18] V. Yu. Dobretsov, I. R. Pankratov, and V. G. Vaks, Pis'ma Zh. Eksp. Teor. Fiz. **80**, 703 (2004). [JETP Lett. **80**, 602 (2004)].

[19] V. Yu. Dobretsov, I. R. Pankratov, A. Yu. Stroev, and V. G. Vaks, Solid→Solid *Phase Transformations in Inorganic Materials 2005* (Ref. 5), Vol. 1, pp. 169–186.

[20] I. R. Pankratov, A. Yu. Stroev, and V. G. Vaks, *Mathematical Modeling and Computer Simulation of Material Technologies*, The Fourth International Conference MMT-2006, Ariel, Israel, 2006, (unpublished) Vol. 1, pp. (I-85)–(I-95).

[21] J. W. Cahn and J. E. Hilliard, J. Chem. Phys. **31**, 688 (1959).

[22] V. G. Vaks, S. V. Beiden, and V. Yu. Dobretsov, Pis'ma Zh. Eksp. Teor. Fiz. **61**, 65 (1995) [JETP Lett. **61**, 68 (1995)].

[23] N. G. Van Kampen, *Stochastic Processes in Physics and Chemistry* (North-Holland, Amsterdam, 1984).

[24] K. Oki, H. Sagane, and T. Eguchi, J. Phys. Colloq. **38**, C7 (1977); K. Oki, S. Matsumura, and T. Eguchi, Phase Transitions **10**, 257 (1987).

[25] H. Tanaka, T. Yokokawa, H. Abe, T. Hayashi, and T. Nishi, Phys. Rev. Lett. **65**, 3136 (1990).

[26] H. Tanaka, Phys. Rev. Lett. **72**, 1702 (1994).

[27] K. D. Belashchenko, G. D. Samolyuk, and V. G. Vaks, J. Phys.: Condens. Matter **11**, 10567 (1999).

[28] V. Yu. Dobretsov and V. G. Vaks, J. Phys.: Condens. Matter **10**, 2261 (1998); **10**, 2275 (1998).

[29] F. Ernst and P. Haasen, Phys. Status Solidi A **104**, 403 (1987).